2016

The erosion response to Quaternary climate change quantified using uranium isotopes and in situ-produced cosmogenic nuclides

Anthony Dosseto
University of Wollongong, tonyd@uow.edu.au

Mirjam Schaller
University of Tubingen

Publication Details

Dosseto, A. & Schaller, M. (2016). The erosion response to Quaternary climate change quantified using uranium isotopes and in situ-produced cosmogenic nuclides. Earth-Science Reviews, 155 60-81.

The erosion response to Quaternary climate change quantified using uranium isotopes and in situ-produced cosmogenic nuclides

Abstract
Studying how catchment erosion has responded to past climate change can help us better understand not only how landscape evolution operates, but also predict the consequences of future climate change on soil resource availability. Recent years have seen the development of tools that allow a quantitative assessment of past changes in catchment erosion. This work reviews the principles of the application of in situ-produced cosmogenic nuclides and uranium isotopes to quantifying past erosion rates. Results highlight the role of periglacial processes and mass wasting in dictating how catchment erosion responds to climatic variability at the 10-kyr scale. At the million-year scale, it is more difficult to untangle the role of climate and tectonics. A strong coupling exists at the 10-kyr to 100-kyr scales between climatic cycles and the transfer time of regolith from source to sink. This coupling reflects changes in sediment source that are either set by changes in vegetation cover at the catchment scale, or by the storage of sediments on continental shelves, at a larger scale. Although further analytical developments are required for these tools to reach their full potential, existing works suggest that in the near future, they will provide unprecedented quantitative insights on how soil and fluvial systems adapt to external perturbations (climatic, tectonic and/or anthropic).

Disciplines
Medicine and Health Sciences | Social and Behavioral Sciences

Publication Details
Dosseto, A. & Schaller, M. (2016). The erosion response to Quaternary climate change quantified using uranium isotopes and in situ-produced cosmogenic nuclides. Earth-Science Reviews, 155 60-81.

The erosion response to Quaternary climate change quantified using uranium isotopes and *in situ*-produced cosmogenic nuclides

Anthony Dosseto[1,]* and Mirjam Schaller[2]

[1] Wollongong Isotope Geochronology Laboratory, School of Earth and Environmental Sciences. University of Wollongong. Northfields Avenue, Wollongong, NSW 2522 Australia.

[2] Department of Geosciences. University of Tübingen. Tübingen, Germany.

* Corresponding author: tonyd@uow.edu.au

Abstract

Studying how catchment erosion has responded to past climate change can help us better understand not only how landscape evolution operates, but also predict the consequences of future climate change on soil resource availability. Recent years have seen the development of tools that allow a quantitative assessment of past changes in catchment erosion. This work reviews the principles of the application of *in situ*-produced cosmogenic nuclides and uranium isotopes to quantifying past erosion rates. Results highlight the role of periglacial processes and mass wasting in dictating how catchment erosion responds to climatic variability at the 10-kyr scale. At the million-year scale, it is more difficult to untangle the role of climate and tectonics. A strong coupling exists at the 10-kyr to 100-kyr scales between climatic cycles and the transfer time of regolith from source to sink. This coupling reflects changes in sediment source that are either set by changes in vegetation cover at the catchment scale, or by the storage of sediments on continental shelves, at a larger scale. Although further analytical developments are required for these tools to reach their full potential, existing works suggest that in the near future, they will provide unprecedented quantitative insights on how soil and fluvial systems adapt to external perturbations (climatic, tectonic and/or anthropic).

1 Introduction

Climate variability is likely to have important consequences on water and soil resources (for instance, Ward et al., 2009). In order to better predict the evolution of these resources, it is essential to understand how erosion at the catchment scale (thereafter referred to as *catchment erosion*) responds to climate change. For instance, the degree of change in hillslope erosion in response to long-term variability in average rainfall (> 100 yr) needs to be quantitatively and spatially constrained in order to assess topsoil loss. Recent numerical models suggest that the soil-landscape response to climate change is non-linear and spatially variable, and that there can be a time lag of tens of thousands of years for the hillslope to adjust to new climatic conditions (Cohen et al., 2013).

Previous studies that have investigated the impact of climate on erosion have drawn diverse conclusions. At a global scale, the increase in sedimentation rates (and thus erosion rates) at 3-4 Ma was explained by a switch from low to high frequency climatic oscillations (Herman et al., 2013; Molnar, 2004; Zhang et al., 2001). In this case, it is not so much the magnitude of climatic parameters such as rainfall that matters, but their variability. When investigating the links between erosion and rainfall, most studies have been pointing toward a positive relationship between the two. Bookhagen et al. (2005b) have shown that during periods of intensified monsoon in the western Himalaya, sediment yield increased by a factor of five compared to modern values. This was explained by an increase in landslide activity, and was observed across both decadal (Bookhagen et al., 2005a) and millennial timescales (Bookhagen et al., 2006; Bookhagen et al., 2005b). Enhanced erosion in the Himalaya during periods of intensified monsoon was also suggested at the Holocene (Clift et al., 2008) and Cenozoic timescales (Clift, 2006), although a strong tectonic control is also recognised in the latter case.

Similar observations have been made in the Andes. For instance, Uba et al. (2007) have shown that sediment accumulation rates increased fourfold during a period of intensified monsoon in the late Miocene. In the Quaternary, Bookhagen and Strecker (2012) observed that erosion rates decreased by an order of magnitude between a humid late Pleistocene and modern-day dry conditions; while landslide activity (and thus sediment supply) has increased during humid periods of the late Pleistocene and the Holocene (Trauth et al., 2000; Trauth et al., 2003). More humid conditions have also been proposed to result in enhanced erosion in other tectonically-active regions such as Taiwan (Hu et al., 2012). Quantitative models also support this relationship and predict higher sediment fluxes under humid conditions (Coulthard et al., 2000; Tucker and Slingerland, 1997). Tucker and Slingerland (1997) have shown that periods of increasing runoff result in more denudation, illustrated in the fluvial system by an expansion of the channel network, and aggradation followed by incision in the main channel. Coulthard et al. (2000) also showed that their model is capable of mimicking the fluvial structure of a catchment in the UK.

Not all studies support a positive relationship between rainfall (or runoff) and erosion.Langbein and Schumm (1958) studied changes in sediment yield at the decadal scale across a broad range of climatic zones in the US. They showed that for rainfall values above a given threshold, the sediment yield decreases as a consequence of increased vegetation density and its role in stabilising slopes. In the Midwestern US (Knox, 1972) and in Texas (Blum and Valastro, 1989), silt deposited during humid periods of the Holocene suggested less energetic streams. Brakenridge (1980) has proposed that erosion was strongest at the beginning of Holocene little ice ages in the US and central Europe, and not during humid periods. In East Africa, Acosta et al. (2015) have shown that humid and more densely vegetated parts of the Kenya Rift flanks display lower denudation rates than sparsely vegetated areas, despite higher median hillslope gradients. At the million-year timescale, Burbank et al. (1993) observed a decrease in erosion during a period of monsoon intensification 8 Myr ago and suggesting an increase in vegetation cover and slope stabilisation as a possible explanation (along with reduced tectonic activity and/or decreased glaciation). Derry and France-Lanord (1996) also proposed a decrease in erosion in the Ganges-Brahamaputra basin 7 Myr ago at a time of monsoon intensification, which they explained as a reduction in the tectonic uplift rate in the Himalaya. Finally, Willenbring and von Blanckenburg (2010) observed no change in the $^{10}Be/^{9}Be$ ratio of oceans over the past 10 Myr. This lack of change was interpreted as evidencing constant weathering fluxes over this period of time and led the authors to question any increase in erosion rates in the late Cenozoic associated with more variable climatic conditions (Zhang et al., 2001).

Quantitative models shed some light on why the erosion response to climate change can be so equivocal: Tucker and Slingerland (1997) showed that the drainage basin response to a change in runoff is non-linear. This is illustrated by recent works that have suggested that a resonance behaviour of the sediment flux exists with the period of the input precipitation signal (Godard et al., 2013; Jerolmack and Paola, 2010). The type of forcing signal can also induce variable responses. If discharge increases, the increase in sediment flux will be amplified by the river (Simpson and Castelltort, 2012). However, if sediment concentration increases without an increase in discharge (e.g. in the case of enhanced landsliding), the increase in sediment flux will be dampened by the river resulting in a low sediment flux at the outlet (Simpson and Castelltort, 2012). Thus, because of the non-linear nature of the erosion response to climate change, looking for a 1-to-1 correspondence between climate state and geomorphic response is a task unlikely to reach a successful outcome. As a result, there is a strong need to be able to directly quantify how erosion has varied in the past, for instance in response to Quaternary climate change.

Past erosion rates can be determined using (i) exhumation rates as a proxy, which are in turn quantified by thermobarometry of metamorphic rocks (e.g. Philpotts, 1990) or thermochronology (e.g. Shuster et al., 2005); (ii) incision into surfaces of known age (Abbott et al., 1997; Burbank et al., 1996); (iii) sedimentation rates into a closed basin (Hinderer and Einsele, 2001) or a marine delta (e.g. Worm et al., 1998); (iv) cosmogenic nuclides (e.g. Granger and Smith, 2000); or (v) river sediment load gauging (e.g. Summerfield and Hulton, 1994). The time resolution of these techniques varies from years (sediment load gauging) to millions of years (thermobarometry). Therefore, not all techniques are suitable to study the links between climate and landscape evolution. Furthermore, sedimentation rate studies can be affected by sediment preservation artefacts known as “Sadler effect” (Sadler, 1981; Willenbring and Jerolmack, 2015). Cosmogenic nuclides and uranium-series isotopes operate at a timescale similar to that of climatic cycles, thus offering the opportunity to study such links (Bierman, 1994; Bierman and Nichols, 2004; Bierman and Steig, 1996; Chabaux et al., 2008; Chabaux et al., 2003; Dosseto et al., 2008a; Dosseto et al., 2008b; Granger and Schaller, 2014; Handley et al., 2013a; Lal, 1991; Lee et al., 2010; Schaller and Ehlers, 2006; Schaller et al., 2004; Schaller et al., 2002; Vigier and Bourdon, 2011; Vigier et al., 2001; von Blanckenburg, 2006). Uranium-series isotopes and *in situ*-produced cosmogenic nuclides (thereafter referred simply as *cosmogenic nuclides*) both record the transfer of weathering products from source to sink (Figure 1). These isotopic techniques have allowed us to determine rates of soil production (e.g. Chabaux et al., 2013; Dosseto et al., 2012; Dosseto et al., 2008b; Heimsath et al., 1997; Ma et al., 2010), catchment-wide erosion rates (e.g. Bierman and Nichols, 2004; Bierman and Steig, 1996; Granger and

Schaller, 2014; von Blanckenburg, 2006), floodplain storage times (Hippe et al., 2012), or the residence time of regolith in catchments (Chabaux et al., 2012; Chabaux et al., 2006; Dosseto et al., 2006a; Dosseto et al., 2006b; Dosseto et al., 2008a; Granet et al., 2010; Granet et al., 2007; Vigier et al., 2005; Vigier et al., 2001; Vigier et al., 2006). These tools have been applied to sedimentary deposits to determine palaeo-erosion rates (Charreau et al., 2011; Granger and Schaller, 2014; Schaller and Ehlers, 2006; Schaller et al., 2004; Schaller et al., 2002) or palaeo-regolith residence times (DePaolo et al., 2012; DePaolo et al., 2006; Dosseto et al., 2010; Handley et al., 2013a; Handley et al., 2013b; Lee et al., 2010).

The aims of this review article are (i) to present how cosmogenic nuclides and uranium isotopes operate at Earth surface and how they can be used to infer palaeo-erosion rates and palaeo-regolith residence times, respectively (see Table 1 for a glossary of the terms used); (ii) to discuss results from cosmogenic nuclides and U isotope studies so far; and (iv) by putting these results in the context of other types of work, to discuss the erosion response to Quaternary climate change. While reviews on each technique already exist (for instance, see recent reviews by Dosseto, 2015; Granger and Schaller, 2014), this work is the first of its kind to comprehensively present the mechanics and limitations of the comminution dating technique and the application of cosmogenic isotopes to palaeo-erosion rates, and discuss how these tools provide insights into the erosion response to Quaternary climate change.

2 Principles

2.1 Comminution dating

Uranium-238 (^{238}U) decays into a series of radioactive products with ^{206}Pb as the final, stable isotopic product. The ^{238}U decay chain is composed of a series of daughter-parent systems where each daughter nuclide is the result of alpha or beta disintegration of the parent nuclide. Here we focus on the top chain of the ^{238}U decay series, in particular ^{238}U and ^{234}U. Uranium-234 is the grand-grand-daughter of ^{238}U, with ^{234}Th and ^{234}Pa as intermediate products.

For any geological system closed for more than a million years, the ^{238}U-^{234}U radioactive system is in *secular equilibrium*, i.e. ^{238}U and ^{234}U activities are equal. The activity of a nuclide is the product of its concentration and decay constant. Thus, if a system is in secular equilibrium, ($^{234}U/^{238}U$) is equal to unity (where parentheses denote activities throughout this article). A variety of geological processes induce fractionation between ^{238}U and ^{234}U, termed *radioactive disequilibrium*. When this occurs, ($^{234}U/^{238}U$) deviates from unity to an extent that depends on (i) the fractionation and (ii) the time elapsed since fractionation for a discrete process, or the rate of fractionation for a continuous process.

Although ^{234}U and ^{238}U have theoretically the same chemical behaviour, as illustrated by the absence of significant fractionation in igneous rocks, fractionation between these two isotopes at the Earth's surface is observed as a consequence of several processes:

1. Direct recoil of ^{234}Th out of the mineral grain during decay of ^{238}U and subsequent decay into its granddaughter ^{234}U (Kigoshi, 1971). When ^{238}U decays into ^{234}Th, the daughter is displaced. This displacement (termed *recoil length*) is between 15 and 35 nm for most minerals (Hashimoto et al., 1985). If this occurs within a recoil length

from the mineral surface, a fraction of ^{234}Th can be lost to the surrounding medium (air or water).

2. Preferential leaching of ^{234}U embedded in recoil tracks (Fleischer, 1980; Fleischer, 1982). A fraction of recoiled ^{234}Th can be embedded into adjacent minerals in recoil tracks, especially when the pore space is filled with air (Sun and Furbish, 1995). The ^{234}U produced can then be easily leached out of the tracks when a solution fills the pore space (Andersen et al., 2009; Fleischer, 1980). Complete leaching of embedded nuclides occurs over a timescale as short as 200 years (Fleischer, 1980).
3. Preferential oxidation of ^{234}U compared to ^{238}U. Computer simulations of the motion of recoiled ^{234}Th have shown that in minerals with a low U content, there is a high probability for ^{234}U to be found in the vicinity of oxygen atoms or radicals (Adloff and Roessler, 1991). As a result, ^{234}U is more prone to oxidation to the hexavalent state, and thus to preferential mobilisation compared to tetravalent ^{238}U.

Initially, it was proposed that by determining the fraction of ^{234}Th directly recoiled out of minerals, one could quantify the supply rate of ^{234}U to the solution leaching these minerals (Kigoshi, 1971). However, it was later postulated that preferential leaching of embedded ^{234}U is another important mechanism for the delivery of ^{234}U to solutions (Fleischer, 1980). It is worth noting that although differentiating both mechanisms is important to accurately study the enrichment of solutions in ^{234}U over ^{238}U, when studying the complementary depletion of ^{234}U in residual solids (as it is the case below), such differentiation is not necessary. Indeed, although the estimation of recoiled ^{234}Th can over-estimate the actual amount of ^{234}U lost if a significant proportion is embedded into adjacent grains, it is exactly because these embedded nuclides are subsequently leached from recoil tracks that eventually all the ^{234}Th recoiled ends up being lost from the minerals; whether directly recoiled in the water or embedded to another grain and later leached.

Because activity ratios are time-sensitive, this allows us to determine time constraints on weathering processes. Early studies investigated qualitatively how to account for radioactive disequilibrium in soils (e.g. Rosholt, 1982; Rosholt et al., 1966). Latham and Schwarcz (1987) and later Scott et al. (1992), developed quantitative models that describe the evolution of nuclide abundances in weathered rock, soil or sediment. In Latham and Schwarcz (1987), an uranium-leach model was proposed to account for (^{234}U/^{238}U) ≤1 in weathered granitic rocks. In this model, the abundance of ^{238}U in the solid material (rock, soil, or sediment) varies with time as follows:

$$\frac{dN_8}{dt} = -w_8.N_8 \tag{1}$$

where N_8 is the number of atoms of ^{238}U and w_8 is a leaching coefficient for ^{238}U (in yr^{-1}; see Table 2 for a definition of all parameters used). Loss of ^{238}U via decay is neglected over the timescales of soil and fluvial processes (<1 Myr).

For ^{234}U, the equation is written:

$$\frac{dN_4}{dt} = \lambda_8.N_8 - \lambda_4.N_4 - w_4.N_4 \tag{2}$$

where N_4 is the number of atoms of ^{234}U, w_4 and λ_4 are the leaching coefficient and decay constant for ^{234}U, respectively (both in yr^{-1}) and λ_8 is the decay constant for ^{238}U (in yr^{-1}).

In Equation (2), it is assumed that all ^{234}U produced by decay of ^{238}U remains in the solid. However, as shown above, a fraction can be ejected via recoil. Scott et al. (1992) proposed a different formulation in order to account for this:

$$\frac{dN_4}{dt} = (1 - f_4)\lambda_8.N_8 - \lambda_4.N_4 - w_4.N_4 \tag{3}$$

where (1 - f_4) represents the fraction of ^{234}U that remains in the solid (Chabaux et al., 2008). Equations (1) and (3) can be used to describe the evolution of ^{238}U and ^{234}U abundances in sediment. The ($^{234}U/^{238}U$) activity ratio is then written:

$$\left(\frac{^{234}U}{^{238}U}\right) = \left(\frac{^{234}U}{^{238}U}\right)_0 .e^{-(\lambda_4 + w_4 - w_8)t} + \frac{(1 - f_4).\lambda_4}{\lambda_4 + w_4 - w_8}\left(1 - e^{-(\lambda_4 + w_4 - w_8)t}\right) \tag{4}$$

where $\left(\frac{^{234}U}{^{238}U}\right)_0$ is the ($^{234}U/^{238}U$) ratio at time $t_0 = 0$, the inception of U isotope fractionation. This equation can be re-arranged to infer the time elapsed since t_0:

$$t_{weath} = -\frac{1}{\lambda_4 + \left(\frac{w_4}{w_8} - 1\right)w_8} \ln\left[\frac{\left(\frac{^{234}U}{^{238}U}\right) - \frac{(1 - f_4)\lambda_4}{\lambda_4 + \left(\frac{w_4}{w_8} - 1\right)w_8}}{\left(\frac{^{234}U}{^{238}U}\right)_0 - \frac{(1 - f_4)\lambda_4}{\lambda_4 + \left(\frac{w_4}{w_8} - 1\right)w_8}}\right] \tag{5}$$

If ^{234}U and ^{238}U are released at the same rate during mineral dissolution ($w_4 = w_8$), then Equation (5) simplifies to:

$$\left(\frac{^{234}U}{^{238}U}\right) = \left(\frac{^{234}U}{^{238}U}\right)_0 .e^{-\lambda_4 t} + (1 - f_4)\left(1 - e^{-\lambda_4 t}\right) \tag{6}$$

This equation describes the evolution of the ($^{234}U/^{238}U$) activity ratio when loss of ^{234}U by recoil is the dominant process fractionating U isotopes. The recoil length in common U-bearing minerals is between 15 and 35 nm (see below) and loss of ^{234}U by recoil occurs when decays takes place within such a lengthscale of a mineral surface. Consequently, this process is only significant when the surface/volume ratio of the mineral is large. Typically, this occurs for grain sizes of a few tens of μm or less. DePaolo et al. (2006, 2012) proposed to use Equation (6) to determine the time elapsed since inception of ^{234}U loss by recoil, termed *comminution age*:

$$t_{comm} = -\frac{1}{\lambda_4}\ln\left[\frac{\left(\frac{^{234}U}{^{238}U}\right)-(1-f_4)}{\left(\frac{^{234}U}{^{238}U}\right)_0-(1-f_4)}\right] \tag{7}$$

Note that DePaolo et al (2006, 2012) denoted the ^{234}U recoil loss fraction, f_α. However, to avoid confusion with the actual α particle produced during decay, and because recoiled nuclides (e.g. ^{230}Th, ^{226}Ra) have different loss fractions, we propose to note the ^{234}U recoil loss fraction f_4 (as in Equation (3)).

In the context of weathering processes, the comminution age represents the time since the parent rock was reduced to fine-grained sediment (or *comminuted*) *via* physical and chemical weathering. Thus, this age encompasses the entire history of regolith at the Earth's surface since its production from the parent rock: storage in the weathering profile, transport in the river with possible temporary deposition in an alluvial plain, and final deposition (in a fluvial terrace, palaeo-channel, lake or oceanic basin; Figure 2). If applied to sedimentary deposits and the age of the deposit is known independently, the difference between the comminution and deposition ages is the *palaeo-regolith residence time* (Figure 2). This residence time indicates for how long the regolith resided in the catchment (hillslope, alluvial transport and storage) before deposition. By applying this approach to sediment with variable deposition ages, it is possible to re-construct variations in palaeo-regolith residence time and thus assess how erosion and fluvial transport have responded to Quaternary climate change. In order to quantify the palaeo-regolith residence time, several conditions need to be met and they are detailed below.

a. Isolation of rock-derived minerals

To determine the comminution age of a soil or sediment, one aims at measuring the ($^{234}U/^{238}U$) ratio of the *rock-derived minerals*. However, in soil and sediment we also find *solution-derived minerals*, i.e. precipitated from a solution (e.g. calcium carbonate, iron oxides and hydroxides), *allogenic minerals* (e.g. aeolian deposits) and organic matter. They need to be removed in order to successfully apply the comminution dating approach. An added difficulty is that any treatment used must not affect the surface properties of rock-derived minerals, because the ^{234}U -^{238}U disequilibrium occurs at their surface.

DePaolo et al. (2006) proposed to apply sequential extraction techniques in order to chemically isolate rock-derived minerals. Because there is no known physical or chemical treatment to isolate aeolian phases, their role on the U isotope ratio of the sediment is generally assessed with mass balance calculations (e.g. Dosseto et al., 2010). Thorough evaluations of the sample preparation for comminution dating were undertaken by Lee (2009) and Martin et al. (2015). It was postulated that the most adapted procedure would be that which produces the lowest ($^{234}U/^{238}U$) ratio in the leached sample (Figure 3) (DePaolo et al., 2012; Lee, 2009; Martin et al., 2015). Following Martin et al. (2015) experiments, the most adequate protocol is a modified version of that from Tessier et al. (1979) and summarised in Table 3. Differences with the procedure of Tessier et al. (1979) are (i) the exclusion of the exchangeable leaching step, as a negligible fraction of U is removed in this step; (ii) the addition of sodium citrate to each step, in order to prevent re-adsorption of U onto the sediment; (iii) the introduction of a final step where the sample is leached with a 0.3M HF-0.1M HCl solution, in order to ensure optimal 'cleaning' of rock-derived phases. Martin et al. (2015) showed that this protocol yields consistent results on various types of material (soil, fluvial and marine sediment).

b. Knowledge of the initial (^{234}U/^{238}U) ratio

Calculation of the comminution age requires knowledge of the (^{234}U/^{238}U) ratio at t=0. When studying soil or fluvial sediment, it is assumed that initial conditions are represented by the unweathered bedrock and that (^{234}U/^{238}U)$_0$ should be equal to 1, because rocks older than 1 Myr are in secular equilibrium. However, this hypothesis is challenged by the observation of ^{234}U-^{238}U disequilibrium in rocks that often show no evidence of chemical weathering (Dosseto and Riebe, 2011; Handley et al., 2013b; Landström et al., 2001; Rosholt, 1983). While plutonic and sedimentary rocks can display (^{234}U/^{238}U) $\neq$ 1, DePaolo et al. (2012) have shown that modern glacial outwash produced from plutonic or sedimentary rocks, has a (^{234}U/^{238}U) = 1. This could suggest that despite variable U isotope composition in parent rocks, the isotopic ratio is "reset" when the rock is weathered into fine-grained sediment.

c. Determination of the recoil loss fraction

Determination of the recoil loss fraction (Equation (3)) is key in order to derive comminution ages. The recoil loss fraction can be estimated using the surface area of the sediment (Kigoshi, 1971; Luo et al., 2000):

$$f_4 = \frac{1}{4} L S \rho \qquad (8)$$

where S is the specific surface area (in m^2/g) and ρ the density (in g/m^3). The specific surface area is generally measured by gas adsorption following the Brunauer-Emmett-Teller (BET) theory (Brunauer et al., 1938), commonly using nitrogen as the adsorbate. However, gas adsorption generally overestimates the recoil loss fraction because it gives a measure of the surface area at a lengthscale several orders of magnitude lower than that of recoil. In order to account for this, Bourdon et al. (2009) proposed to use the fractal model initially developed by Semkow (1991). In this model, the recoil loss fraction is written as follows:

$$f_4 = \frac{1}{4}\left[\frac{2^{D-1}}{4-D}\left(\frac{a}{L}\right)^{D-2}\right]LS\rho \qquad (9)$$

where D is the fractal dimension of the surface and a is the size of the adsorbate molecule (0.354 nm for nitrogen). The fractal dimension D is a measure of the surface irregularities. It is in essence similar to the surface roughness, λ_s. It can vary between 2 and 3, where 2 corresponds to a perfectly smooth surface (i.e. $\lambda_s = 1$) and 3 relates to a maximum surface complexity (or $\lambda_s \rightarrow \infty$). The fractal dimension is determined using BET surface area measurements: in a diagram showing the logarithm of the quantity of gas adsorbed as a function of the double logarithm of the relative pressure, the slope equals *D - 3* (Avnir and Jaroniec, 1989).

Using Equation (9) to estimate the recoil loss fraction, Aciego et al. (2011) have shown that it is possible to successfully date ice core samples by measuring the excess ^{234}U supplied to the ice by recoil of ^{234}Th from trapped dust particles. At this stage of development of the comminution dating technique, estimating the recoil loss fraction using the surface area and fractal dimension appears to be the best available approach since both parameters can be determined by gas adsorption and BET theory. If these parameters can be accurately determined, the resulting uncertainties on the comminution age are typically up to 20-25 % at 2σ level (Handley et al., 2013a).

d. Recoil length of various minerals

Estimation of the recoil loss fraction requires knowledge of the ^{234}Th recoil length. This length is generally assumed to be 30-40 nm (DePaolo et al., 2006; Maher et al., 2006a), whilst in zircon it can be as short as 23 nm (Ziegler et al., 1996) (Table 4). Choosing a recoil length between 28 and 32 nm induces an uncertainty of about 5% (at 2σ level) on the calculated comminution age (Handley et al., 2013a). The recoil length can be calculated using the SRIM computer model based on the binary collision approach developed by Ziegler et al. (1996):

$$L_{bulk} = \sum_j \frac{m_j U_j}{U_{bulk}} L_j \qquad (10)$$

where L_{bulk} and L_j are the ^{234}Th recoil lengths in the bulk material and mineral j, respectively. m_j is the mass fraction of mineral j. U_{bulk} and U_j are the U concentrations in the bulk material and mineral j, respectively. For instance, if we consider sediments composed of 60% quartz, 39% muscovite and 1% zircon, where the U concentrations in the quartz, muscovite and zircon are respectively 0.1, 1 and 100 ppm, the bulk recoil length is 22 nm.

e. Change in surface properties during transport

In Equation (3), it is assumed that the recoil loss fraction f_4 is constant with time. In other terms, because f_4 is a function of the surface area and roughness, this means that the surface properties of the sediment are assumed constant with time. Obviously, this is unlikely to be the case since size reduction from bedrock to soil/sediment must be accompanied by changes in surface properties. To address this, we can use Equation (9) to model how the recoil loss fraction may vary with time. We assume that the fractal dimension varies linearly between 2 (t = 0, when the sediment particle is detached from the bedrock) and 3 (t = T_{max}, the amount of time required to obtain a particle with the maximum roughness allowed by the fractal dimension). The surface area is arbitrarily assumed to vary linearly between S_0 = 1 and S_{max} = 100 m^2/g, which encompasses values typically measured for minerals and sediment. We modelled f_4 for different values of T_{max}: 0.1, 1 and 10 Myr (Figure 4). Using a recoil length of 30 nm and a density of 2650 kg/m^3, f_4 increases from ~0.02 to peak at ~0.1 after about 0.1xT_{max}. The modelled f_4 evolution can then be used to calculate how the ($^{234}U/^{238}U$) of the sediment would evolve with a time-dependent recoil loss fraction. This in turn can be used to calculate the difference between the comminution age calculated considering a constant f_4 (*apparent comminution age*) and that calculated using a time-dependent f_4 (*true comminution age*). Results are shown on Figure 5 for T_{max} = 1 Myr. Assuming a constant f_4 leads to gross overestimations of the age for sediment younger than 20 kyr (i.e. true comminution age < 20 kyr). However, for sediment with a comminution age between 20 and 500 kyr, the uncertainty introduced by assuming a constant recoil loss fraction is less than 30%, thus yielding satisfying estimates of the comminution age.

f. Preferential leaching of ^{234}U

Two mechanisms have been invoked to account for ($^{234}U/^{238}U$) >1 in natural waters: direct recoil of ^{234}Th and subsequent decay into ^{234}U (Kigoshi, 1971), and preferential leaching of ^{234}U embedded in recoil tracks (e.g. Fleischer, 1980; Hussain and Lal, 1986). Dissolution experiments performed on a freshly ground granite showed that solutions exhibit ($^{234}U/^{238}U$) >1 after only a few 10's-100's hours of water-rock interaction (Andersen et al., 2009). Because minerals did not have time to develop ^{234}U depletion from direct recoil (which requires several 10's of kyr), these results emphasized the importance of ^{234}U preferential leaching in imparting natural waters with a ($^{234}U/^{238}U$) >1. When considering the ^{234}U -^{238}U isotope composition of the solid residue, it is important to take into account the timescales over which preferential leaching and direct recoil operate: Fleischer (1980) reported that after only 1 week of exposure of recoil tracks to solutions, 50% of the embedded ^{234}U would be leached out. Thus, after 200 years all the ^{234}U available for preferential leaching would have been removed. Because the comminution age integrates fluvial transport and storage in weathering profiles, ages are expected to be greater than several thousand years in most cases. Consequently, preferential leaching of ^{234}U is likely to be negligible over these timescales. However, this is only true for embedded tracks exposed at T=0. The scenario where recoil tracks are continuously exposed as a result of mineral dissolution is discussed below.

g. Effect of mineral dissolution

As indicated above, Equation (7) assumes that ^{234}U-^{238}U fractionation is controlled by the loss of ^{234}U via recoil. However, if mineral dissolution occurs during sediment transfer, additional fractionation can take place if ^{234}U and ^{238}U are released at different rates as a result of mineral breakdown ($w_4 \neq w_8$). This can occur via (i) leaching of ^{234}U embedded in recoil tracks exposed by mineral dissolution and/or (ii) preferential oxidation of ^{234}U to the hexavalent state as a result of ^{234}Th recoil (Adloff and Roessler, 1991). The latter may be insignificant considering that at the Earth's surface ^{238}U is in most cases in the hexavalent state too. DePaolo et al. (2006) proposed that the effect of dissolution could be evaluated by comparing the timescale to develop ^{234}U depletion by recoil, τ_{recoil}, to the timescale for dissolution to remove a layer of thickness equivalent to one ^{234}Th recoil length, τ_{diss}:

$$\frac{\tau_{recoil}}{\tau_{diss}} = \frac{R}{\lambda_4 L \rho} \qquad (29)$$

where R is the mineral dissolution rate. Using L = 30 nm, ρ = 2700 kg/m^3 and R = 2.5 x 10^{-18} mol/m^2/s, they calculated that this ratio would be only 0.1, suggesting that dissolution has a minor role on the (^{234}U/^{238}U) ratio. However, the mineral dissolution rate they considered (calculated for plagioclase in Maher et al., 2006b) is much lower than values compiled for various common minerals (White and Brantley, 2003): between 10^{-17} and 10^{-13} mol/m^2/s for field-based weathering rates. Consequently, dissolution could have a greater impact on the sediment (^{234}U/^{238}U) ratio than proposed by DePaolo et al. (2006). This impact can possibly be accounted for if Equation (3) is re-written as follows:

$$\frac{dN_4}{dt} = (1 - f_d)(1 - f_4)\lambda_8 N_8 - \lambda_4 N_4 - w_4 N_4 \tag{11}$$

where f_d is the fraction of ^{234}U that is released from newly exposed recoil tracks during dissolution. In this case, the comminution dating equation would be written as:

$$t_{comm} = -\frac{1}{\lambda_4} \ln\left[\frac{\left(\frac{^{234}U}{^{238}U}\right) - (1 - f_d)(1 - f_4)}{\left(\frac{^{234}U}{^{238}U}\right)_0 - (1 - f_d)(1 - f_4)}\right] \tag{12}$$

The parameter f_d is a function of the dissolution rate and the surface area of the mineral. However it is yet to be characterised. Future work should aim at achieving this so the ^{234}U-^{238}U fractionation is fully constrained. Nevertheless, as shown below, while preliminary studies have investigated the limitations of the technique, they have also highlighted its potential, bringing new insights on the relationships between Quaternary climate change and fluvial dynamics.

2.3 In situ-produced cosmogenic nuclides: quantification of modern and past catchment-wide erosion rates

a. Catchment-wide erosion rate

Cosmic rays (protons and neutrons) penetrate the atmosphere and produce a cascade of secondary rays (neutrons and muons). This shower of secondary rays bombards the Earth surface, producing cosmogenic nuclides *in situ*, i.e. within the crystal structure of minerals (e.g. Gosse and Phillips, 2001). For example, spallation of ^{16}O in quartz produces ^{10}Be (Lal, 1991), while spallation of Ca isotopes in plagioclase or calcite produces ^{36}Cl (Stone et al., 1996). Thus, the type of nuclide produced depends on the target mineral. *In situ*-produced cosmogenic nuclides (cosmogenic nuclide), whether radioactive (^{10}Be, ^{14}C, ^{26}Al, ^{36}Cl) or stable (^{3}He, ^{21}Ne, and ^{22}Ne), are used in many geological applications to quantify Earth surface processes. At Earth surface, the measurement of ^{10}Be (half-life, $t_{1/2}$ = 1.387 Myr) and ^{26}Al ($t_{1/2}$ = 0.702 Myr) in sediment, soils or rocks is often used to quantify *erosion rates* (i.e. the combined rates of physical and chemical transport of weathering products; often termed *denudation rates*). These two nuclides are commonly used because they are produced in the relatively weathering-resistant and ubiquitous mineral quartz. Hence, loss of nuclides out of the mineral lattice due to weathering and diffusion should be minimal. The mineral needs to be a closed system for a successful denudation rate determination. In addition, due to the simple chemistry of quartz, the production rates of ^{10}Be and ^{26}Al are relatively well constrained. The production rate is a function of the geomagnetic field intensity over space and time, mineral composition, shielding by topography, vegetation or snow cover, and absorption of cosmic rays in rock and soil. The depth dependence of the cosmogenic nuclide production is known whereby production by nucleons dominates at shallow depths, while fast and stopped muons are the main agent of production at greater depths (e.g. Braucher et al., 2003; Figure 6). If the production rate of an cosmogenic nuclide is known and its concentration can be measured, then the erosion rate of a steadily eroding surface can be determined (Lal, 1991). At steady-state, the production of cosmogenic nuclides equals the nuclide loss from denudation and radioactive decay. Thus, the nuclide concentration of an eroding material (in atoms.g^{-1}) can be written as:

$$C = \frac{P_{(0)}}{\left(\lambda + \frac{\varepsilon\rho}{\Lambda}\right)} \tag{13}$$

where $P_{(0)}$ is the production rate of the nuclide in a mineral of known composition (in atoms.g^{-1}.yr^{-1}), λ the nuclide decay constant (in yr^{-1}), ε the erosion rate (cm.yr^{-1}), ρ the density of the material (in g.cm^{-3}), and Λ the attenuation length (in g.cm^{-2}), which describes the depth-dependence of the production rate. The production rate needs to take into account production by nucleons, stopped and fast muons. Note that the erosion rate is inversely proportional to the measured nuclide concentration.

In order to determine the erosion rate of an entire landscape, a large number of bedrock samples from across the landscape would need to be analysed. Unfortunately, this process would be very time consuming and expensive. The cosmogenic nuclide concentration of fluvial sediment can be used instead, because rivers average erosion at the catchment scale and therefore provide a representative sample of the entire catchment (e.g. Bierman and Steig, 1996; Brown et al., 1995; Granger et al., 1996). The cosmogenic nuclide concentration of river sediment can be used together with an average of the nuclide production rate over the catchment area to determine a catchment-wide erosion rate. The cosmogenic nuclide-derived erosion rate averages over a certain time scale, which is a function of the erosion rate itself. The averaging time scale is reported as “apparent age” and is based on the time it takes to erode the top 60 cm of rock (von Blanckenburg, 2006). In an active mountain range eroding at 1,000 mm/kyr, the cosmogenic nuclide-derived erosion rate integrates the last 800-900 years. In contrast, in slowly eroding shields and cratons (~1 mm/kyr) it integrates the last 600,000 years.

In order to determine a catchment-wide erosion rate from cosmogenic nuclide measurements, several assumptions need to be verified (Bierman and Steig, 1996; von Blanckenburg, 2006):

1. The sediment cosmogenic nuclide budget is in steady-state at the catchment scale (*isotopic steady-state*): the input of cosmogenic nuclide via *in situ* production over the entire catchment area equals the output of cosmogenic nuclide via sediment export by the river and radioactive decay. This assumption may be invalid in landscapes where mass wasting is important. Another implication of the above requirement is that if the erosion rate changes over time, the cosmogenic nuclide budget needs time to adjust to this new rate. Thus, the cosmogenic nuclide-derived erosion rate can lag behind the true erosion rate (e.g. Schaller and Ehlers, 2006; discussed below).
2. Each eroding area contributes quartz material to the river sediment. If an eroding area does not contribute any quartz, this area should not be included in the production rate calculation. The calculated cosmogenic nuclide-derived erosion rate can be corrected for the non-uniform distribution of quartz due to lithologic variations within a catchment (e.g. Safran et al., 2005).
3. Nuclide concentration is homogeneous across different grain size fractions. If the nuclide concentration varies between different grain size fractions, the difference can be attributed to different transport mechanism (e.g. Brown et al., 1995; Codilean et al., 2012; Matmon et al., 2003b) or different sediment sources (e.g. Wittmann et al., 2010). For

instance, finer grain sizes could be transported over a longer distance than coarser grained material, representing a source area with lower erosion rates.

4. No quartz enrichment occurs in the sediment source area during weathering and erosion processes. If this occurs and the enrichment is not accounted for in the erosion rate calculation, this will lead to an underestimation of the erosion rate (Riebe et al., 2001). However, in most settings the difference between corrected and uncorrected erosion rates is small.
5. Minimal sediment storage takes place in the drainage system (e.g. Matmon et al., 2003a). If sediment is deposited during transport, additional cosmogenic nuclides might be produced by irradiation after deposition, or lost by radioactive decay if storage is deep (Clapp et al., 2002). Model simulations of the cosmogenic nuclide concentrations during transport in a river system have been used to illustrate the possible influence of storage on measured nuclide concentrations (Lupker et al., 2012; Wittmann and von Blanckenburg, 2009). Measurement of an additional radioactive or stable cosmogenic nuclide can help shed further light on storage and remobilization (Wittmann et al., 2011).
6. The time scale of erosion is shorter than the cosmogenic nuclide half-life. The time scale of erosion is given by the time it takes to erode 60 cm of rock. This lengthscale is derived from the attenuation length of cosmic rays (~160 $g.cm^{-2}$) and the exponential nature of the decrease in production rate with depth. The lower the erosion rate, the higher the time scale of erosion. In the case of ^{10}Be in quartz, erosion rates larger than 0.03 mm/kyr can generally be determined (e.g. von Blanckenburg, 2006).
7. Landscapes are often affected by landslides and debris flows, where material shielded at depth is uncovered and supplied to the river. To account for this effect and accurately

determine long-term erosion rates with cosmogenic nuclide, larger catchment areas need to be sampled as the frequency of landsliding increases (Niemi et al., 2005). For instance, samples integrating drainage areas larger than 100 km^2 need to be collected where deep landslides (>5 m) are common (Yanites et al., 2009).

8. Shielding by glaciers, snow, and vegetation in the sediment source area is not significant. If shielding is significant, production rates used in calculations need to be corrected for shielding (Delunel et al., 2014; Godard et al., 2012; Schildgen et al., 2005). In the case of glaciation, the production rate for the catchment area covered by glaciers is generally assumed to be zero. In the case of snow and vegetation shielding, the production rate is reduced. This reduction in production rate results in a lower calculated erosion rate than if no correction was applied.

In many settings, violations of these assumptions are not avoidable and their possible influence on calculated erosion rates needs to be addressed. One important assumption often violated is that of isotopic steady-state. After a change of erosion rate, the isotopic system is disturbed and needs time to adjust to the new conditions. Therefore, variations in actual erosion rates are smoothed out and/or delayed in time (Bierman and Steig, 1996; von Blanckenburg, 2006). For instance, a tenfold increase in erosion rate from 30 to 300 mm/kyr over a 100 year time period is not detectable in the cosmogenic nuclide signal. In contrast, a tenfold increase over 100,000 years (one climatic cycle in the late Pleistocene) allows enough time for the system to reach steady-state again (e.g. Schaller and Ehlers, 2006). Schaller and Ehlers (2006) modelled how cosmogenic nuclide-derived erosion rates compare to true time-dependent erosion rates (Figure 7). Input (true) erosion rates were generated for different mean values (10, 100, and 1000 mm/kyr), periodicity (23, 41 and 100 kyr) and amplitude (0.1, 0.5, and 1.0) (Figure 7). When input erosion rates have a high mean value (>500 mm/kyr) and changes occur with a long periodicity (e.g. 100 kyr), cosmogenic nuclide-derived erosion rates closely follow true rates. In addition, the assumption of minimal sediment storage and remobilisation in the catchment needs to be addressed. During storage in alluvial deposits, the sediment nuclide budget can increase through post-depositional irradiation (shallow burial) or decrease through decay (deep burial; Clapp et al., 2002). Short-lived isotopes such as in situ-produced ^{14}C in quartz can be used to eliminate floodplain sediment storage times (Hippe et al., 2012). However, for long-lived isotopes (e.g. ^{10}Be and ^{26}Al) it has been shown that the effect of storage and remobilisation is often minor and the cosmogenic nuclide concentration is relatively constant over large distances (Lupker et al., 2012; Wittmann and von Blanckenburg, 2009). As nuclide concentration does not shift in large flood plains, it is assumed that nuclide concentration records the erosion rate in the sediment source area. Hence, the average production rate in the sediment source area is used. The use of the average production rate from the sediment source area rather than that from the enitre catchment is known as the concept of *floodplain correction* (e.g. Wittmann et al., 2009). In addition, this sediment storage and remobilisation induces further delaying and damping of the erosion rate signal which already exist due to climatic and tectonic variations of erosion rates (e.g. Davis et al., 2012).

Over the last 25 years, applications based on cosmogenic nuclide have expanded at a rapid rate (Granger et al., 2013). Portenga and Bierman (2011) compiled and re-calculated over a thousand cosmogenic nuclide-derived catchment-wide erosion rates, seeking correlations with a wide range of parameters (latitude, elevation, relief, mean annual precipitation and temperature, seismicity, basin slope and area, and vegetation cover). Mean basin slope appears to be the main control on erosion rates in landscapes with slopes >200 m/km (e.g., Carretier et al. (2013). In another study, erosion rates derived from cosmogenic nuclide measurement (10-kyr timescale) and stream gauging (10-yr timescale) were compared (Covault et al., 2013). It was shown that in most cases, cosmogenic nuclide-derived rates were greater than corresponding stream gauge-derived rates. This was attributed to the low frequency-high magnitude nature of sediment transport events. Nevertheless, stream gauge-derived rates were in the same order of magnitude as cosmogenic nuclide-derived rates, which was explained by the buffering capacity of large flood plains.

b. Palaeo-erosion rates

The cosmogenic nuclide signal acquired during catchment erosion in the sediment source area is stored in sedimentary deposits such as cave sediment, river terraces, palaeo-channels, or deltas (e.g. Granger and Schaller, 2014). The measured nuclide concentration in sediment archives (C_{tot}) is a composite of the concentration inherited from the palaeo-erosion rate (C_{in}) corrected for decay over time and the amount of nuclides produced after sediment deposition (C_{dep}) (Anderson et al., 1996):

$$C_{tot} = C_{in} e^{-\lambda t} + C_{dep} \qquad (14)$$

where λ is the decay constant of the cosmogenic nuclide (in yr^{-1}) and t is the time elapsed since sediment deposition (in yr) (Table 5). C_{in} is given as C in Equation (13) and the production rate is the catchment-average production rate of the sediment source area. C_{dep} is given by:

$$C_{dep} = P_{(0)} e^{\frac{x\rho}{\Lambda}} \frac{1-e^{-\lambda t}}{\lambda} \qquad (15)$$

where $P_{(0)}$ is the production rate at the sampling site (in atoms.$g_{(qtz)}^{-1}$.yr^{-1}), x the depth of burial (in cm), ρ the density of the sediment (in g.cm^{-3}), and Λ is the attenuation length (g.cm^{-2}) (Table 5). All production mechanisms (neutrons, stopped and fast muons) need to be taken into account. In order to apply this approach to sedimentary deposits, several requirements need to be met in addition to those presented above for modern river sediments:

1. The age of the deposit is known. After deposition, the nuclide concentration changes over time due to decay and post-depositional irradiation. Hence, the age of the sedimentary deposit needs to be determined independently, such as through the use of ^{14}C, optically-stimulated luminescence (OSL) dating, U-series, dating of ash layers, palaeo-magnetostratigraphy, fossil assemblages, or cosmogenic nuclides (e.g. depth profile dating, simple burial dating, isochron burial dating).
2. Sediment deposition is fast and the history of burial depth over time can be inferred in order to correct for post-depositional irradiation.
3. Post-depositional irradiation is small enough such that the inherited nuclide concentration dominates the nuclide budget (e.g. Balco and Stone, 2005). Post-depositional irradiation can be kept to a minimum by collecting well-shielded samples (e.g. caves, deltas, deep sedimentary sequences) or young sediment deposits (e.g. Granger and Muzikar, 2001). For instance, a deep or short burial is required when the erosion rate is high in the sediment source area, as high erosion rates only impart a low cosmogenic nuclide concentration to sediments.

4. Changes in the catchment-wide production rate due to changes in catchment area and elevation are known. Generally, it is assumed that the catchment-wide production rate used for calculation of palaeo-erosion rate is the same as at present (e.g. Schaller et al., 2002). However, the production rates can be significantly affected by tectonic activity and/or river capture, thus influencing the calculated palaeo-erosion rate. The evolution of a river system over time needs to be well constrained.

Meeting all these requirements can be challenging and the application of the cosmogenic nuclide technique in natural settings needs to be carefully evaluated. For instance, the correction for nuclide decay and post-depositional irradiation requires knowing the sediment deposition age and history (e.g. burial depth over time). Fortunately, deposition ages can be constrained using different techniques (e.g. luminescence, radiocarbon, U-series, cosmogenic nuclide dating).

As an example, different cosmogenic nuclide approaches can be used to determine clastic sediment deposition ages: depth profile dating (e.g. Granger and Smith, 2000), simple burial dating (Granger et al., 1997) or isochron burial dating (e.g. Balco and Rovey, 2008). Simple burial dating can be applied in sediment deposits protected from post-depositional irradiation (e.g. cave sediment, deltas). It makes use of the different half-lives of ^{26}Al and ^{10}Be and the knowledge of the production ratio of these two isotopes at the Earth surface (e.g. Granger, 2014; Granger and Muzikar, 2001). Once sediments are deposited in a cave and protected from further irradiation, the cosmogenic nuclide clock starts ticking. The older the sediment burial, the lower the measured ^{26}Al/^{10}Be ratio as ^{26}Al decays faster than ^{10}Be. Unfortunately, post-depositional irradiation cannot always be excluded and simple burial dating may not be applicable. In such cases, the determination of sediment deposition ages can be attempted by depth profile or isochron burial dating. The former is based on the analysis of several sediment samples from different depths in the deposit (e.g. Granger and Smith, 2000). By measuring the nuclide concentrations at different depths, the deposition age, erosion rate and inherited nuclide concentration can be determined. In contrast, the isochron burial technique makes use of several clast samples from the same depth (e.g. Erlanger et al., 2012). The clast samples need to be analysed for both ^{26}Al and ^{10}Be. In a diagram of ^{26}Al vs ^{10}Be concentrations, coeval samples define a line (*isochron*), whose slope contains information about the deposition age (Figure 8). This burial time is independent from the post-depositional erosion history of the terrace. Once the deposition age is determined from the clasts, a sand-sized sample collected from the same depth provides information about the inherited nuclide concentration and thus the palaeo-erosion rate in the sediment source area. The disadvantage of depth profile and isochron burial dating is the relatively large number of sample analysed required, which makes these approaches labour intensive and expensive.

c. Analytical techniques

Samples collected in the field are dried in the laboratory and a specific grain size fraction is retained (e.g. 0.5 – 1.0 mm). Quartz is isolated by magnetic separation, heavy liquids, froth flotation, and dilute hydrofluoric acid treatment (Kohl and Nishiizumi, 1992). The hydrofluoric acid is not only used to destruct feldspar, but also to remove any meteoric ^{10}Be, which is abundant at the mineral surface. Ten to a hundred grams of quartz are dissolved with concentrated hydrofluoric acid. After the addition of a known amount of ^{9}Be carrier and sub-sampling an aliquot for ^{27}Al concentration determination, Al and Be are separated from other elements by precipitation and chromatographic techniques. The clean Al- and Be-hydroxide fractions are then heated to form oxides. Samples are finally sent to dedicated accelerator mass spectrometer facilities and $^{10}Be/^{9}Be$ and $^{26}Al/^{27}Al$ ratios measured (e.g. Christl et al., 2014). With the knowdlege of the $^{10}Be/^{9}Be$ ratio and the ^{9}Be carrier amount, the ^{10}Be concentrations can be calculated. The ^{27}Al concentrations needed for the calculation of ^{26}Al abundances are measured by optical emission or mass spectrometry as well as atomic absorption spectroscopy.

In order to calculate erosion and palaeo-erosion rates from the determined nuclide concentrations, the following parameters need to be constrained:

1. The production rate at sea level and high latitude (SLHL). As production varies over space and time due to magnetic field variability, a SLHL production rate is commonly reported. The production rate of each cosmogenic nuclide needs to be determined individually for a given mineral and production mechanism (e.g. spallation, fast and stopped muons). Absolute production rate values are based on numerical simulations (Masarik and Reedy, 1995) or measurements in material of independently known surface exposure ages (Nishiizumi et al., 1989). Scaling the production rate from the calibration locality to SLHL can be done with various methods (see below), which results in a range of SLHL production rates (Balco et al., 2008; Putnam et al., 2010).
2. Production rate scaling to altitude and latitude. The intensity of cosmic rays, hence the production rate at the Earth surface, varies with the geomagnetic field and the air pressure. The intensity of cosmic rays at sea level is highest at latitudes above 60° and lowest at the equator. The intensity of cosmic rays also increases with decreasing air pressure (i.e. increasing altitude). Different scaling mechanisms for the determination of production rates at different altitude and latitude have been suggested (Desilets et al.,

2006; Dunai, 2000; Lal, 1991; Lifton et al., 2005; Stone, 2000) and applied in the CRONUS-Earth online calculator (Balco et al., 2008).

3. Production rate over time: the strength of Earth's geomagnetic field changes over time, and thus the intensity of cosmic rays influencing the production rates (e.g. Masarik et al., 2001). This variability needs to be taken into account for present-day and palaeo-erosion rate determinations.
4. Depth dependence of the production rate: cosmic rays bombarding Earth surface are slowed down and absorbed. The deeper the penetration, the lower the production rate. The relationship between production rate and depth is a function of the density of the material and the absorption mean free path (e.g. von Blanckenburg, 2006). Different laws of depth dependence for the different production mechanisms are available (Granger and Smith, 2000; Schaller et al., 2001).
5. Production rate shielding: the intensity of cosmic rays is not only affected by the geomagnetic field, but is also reduced by shielding from topography, snow and/or vegetation cover. These shielding effects need to be taken into account when ages and palaeo-erosion rates are determined (e.g. Dunne et al., 1999; Schildgen et al., 2005).

Nuclide measurements and the determination of all these parameters are affected by uncertainties. Taking into account these uncertainties may result in errors as high as 35% for catchment-wide denudation rate determinations (e.g. Lupker et al., 2012; Wittmann et al., 2007). In the case of palaeo-denudation rate determinations, the expected errors may be even higher because additional corrections are required.

3 Applications

3.1 Comminution ages and regolith residence times

The use of uranium isotopes to quantify the comminution age of clastic sediment was first mentioned in Maher et al. (2004) and later applied to deep-sea sediment in DePaolo et al. (2006) to determine palaeo-regolith residence times (termed *transport times* in their study). The ($^{234}U/^{238}U$) activity ratios were measured in drill core sediment at ODP Site 984A, off the south coast of Iceland. Samples were leached in 1.5M HCl to remove carbonates, as a sodium acetate leach was found to be inefficient (Maher et al., 2004).

The recoil loss fraction was not directly quantified, but instead derived graphically: in a diagram showing ($^{234}U/^{238}U$) versus $1-e^{-\lambda_4 t}$, if data form a linear trend, the intercept with $1-e^{-\lambda_4 t}=1$is equal to $1-f_4$. The authors identified two populations of sediment on the basis of their Nd, Sr and U isotopic compositions. This was interpreted as two sediment sources (Iceland and continental Europe) whose contribution varied over time with climatic cycles. From these, DePaolo et al. (2006) determined graphically two f_4 values (Figure 9.) and regolith residence times between 0 to 400 kyr were calculated. Variations in residence times were found to follow climatic cycles (Figure 10) and interpreted to reflect changes in sediment sources: during interglacials, sediment was mostly derived from nearby Iceland, as illustrated by high ε_{Nd} values, low $^{87}Sr/^{86}Sr$ isotopic compositions and short residence times. Conversely, during glacial periods, sediment was mostly derived from continental Europe, as shown by low ε_{Nd} values and high $^{87}Sr/^{86}Sr$ isotopic compositions. Long residence times (300-400 kyr) during glacial periods were explained as continental shelves were exposed and eroded, mobilising sediment stored there for several 100's of kyr.

Dosseto et al. (2010) studied palaeo-channels of the Murrumbidgee River in southeastern Australia, with deposition ages spanning over the last glacial cycle (Banerjee et al., 2002; Page et al., 1996). The recoil loss fraction was estimated by using the grain size distribution for each sample quantified by laser diffraction. Inferred f_4 values (0.025-0.14) were lower than those estimated in DePaolo et al. (2006), ranging from 0.06 to 0.12. This could reflect the different environments investigated in both studies (continental deposits in Dosseto et al. 2010 versus deep-sea deposits in DePaolo et al. 2006), although the large uncertainties in estimating f_4 values in both cases commands caution in making such interpretations.

For the Murrumbidgee River palaeo-channels, Dosseto et al. (2010) inferred residence times varying between 27 ± 8 and 420 ± 78 kyr (Figure 11). Similarly to DePaolo et al. (2006), they observed a cyclicity of residence times with climatic variability: low values (≤100 kyr) during Marine Isotope Stage (MIS) 2, in contrast with high values (>200 kyr) for MIS 1 and 5. These variations were interpreted as reflecting changes in sediment provenance: active hillslope erosion in the headwaters during MIS 2 versus re-working of alluvial deposits during MIS 1 and 5. These changes were in turn explained by the role of vegetation cover on erosion: woodlands dominated the Murrumbidgee headwaters during MIS 1 and 5, inhibiting hillslope erosion, in contrast to shrub-like vegetation during MIS 2 (Kershaw et al., 2007).

In Lee et al. (2010), the comminution dating technique was tested on alluvial deposits from the Kings River Fan (California, USA). It was postulated that the deposition age of sediment must be equal to its comminution age because it is derived from glacial outwash and thus the residence time must be very short. Comminution ages were calculated for different grain size fractions (<6, 10-15, 15-20 and >20 μm). Calculated ages were much younger than theoretical values (i.e. deposition ages). Lee et al. (2010) noted that to reconcile this discrepancy, surface roughness values would need to increase with grain size. However, unless surface roughness can be quantified for different grain size, there is little prospect to use this parameter to determine comminution ages. An alternative approach could have been to determine recoil loss fractions using surface area measurements and fractal dimension determination as in equation (9), but this was not done. While the study by Lee et al. (2010) represented an interesting approach to test the comminution dating technique, it could not provide any insight on past fluvial dynamics since the initial assumption was that all samples studied were characterised by negligible residence times.

Handley et al. (2013a; 2013b) have studied sedimentary deposits of Central and South Australia. In each case, it was difficult to obtain meaningful comminution ages. Possible reasons are (i) incomplete isolation of rock-derived minerals and (ii) a dominant role of aeolian material in these environments. Martin et al. (2015) have shown that existing sequential extraction protocols do not result in a complete removal of organic and solution-derived phases. While the method by Schultz et al. (1998) used in Handley (2013a; 2013b) showed good prospects, a final step with a dilute HF-HCl solution is needed. Furthermore, the role of aeolian material needs to be addressed, as it cannot be removed mechanically or chemically. In order to obtain robust comminution ages, it is recommended that study sites are chosen where aeolian deposition is minimal, or to constrain the U isotope composition of this component.

In summary, the comminution dating technique is still in its infancy and this is illustrated by the difficulty to obtain meaningful ages in some cases. Nevertheless, some preliminary studies have shown that palaeo-regolith residence times are strongly coupled to Quaternary climatic cycles: they record changes in sediment provenance in response to climatic variability, whether at the scale of oceanic basins (DePaolo et al., 2006) or the catchment scale (Dosseto et al., 2010).

3.2 Palaeo-erosion rates

Below we review the application of in-situ cosmogenic ^{10}Be to determine palaeo-erosion rates in the time span of a) the Last Glacial Maximum (LGM) to present and b) the Quaternary Period.

Last Glacial Maximum to present:

Several studies have investigated how palaeo-erosion rates in Europe, North and South America have varied since the late Pleistocene by measuring cosmogenic nuclide in sediment deposited in fluvial terraces. Fuller et al. (2009) applied this approach to strath terraces of the Eel River in northern California (USA), where deposition ages were independently constrained by OSL dating and span from the Late Pleistocene (30 kyr old) to the Holocene. Palaeo-erosion rates derived from the Late Pleistocene terraces are ~30 mm/kyr. These rates are twice as high as those derived from modern river sediment and 3.5 times higher than the rates from terraces deposited at the Pleistocene-Holocene transition (Figure 12). It was thus proposed that the time of fastest erosion and strath planation was coupled with a period of increased precipitation in the late Pleistocene. Furthermore, incision rates based on the terrace height and OSL dating are 2 to 4 times higher than palaeo-erosion rates over the same time period. This suggests an increase in topographic relief of ~300 mm/kyr over the past 20 kyr.

Marshall et al. (2015) have investigated cosmogenic nuclides in lake deposits of Little Lake in the Oregon Coast Range (USA). The lake sediments reveal a palaeo-erosion rate of ~200 mm/kyr at around 23 kyr (Figure 12). This suggests a 2.5 times increase in erosion rates compared to values derived from the modern sediment load. This was attributed to pervasive frost-driven sediment production during the last glacial time in the unglaciated study area.

Schaller et al. (2002) determined cosmogenic nuclide-derived palaeo-erosion rates from fluvial terrace sediment of the Allier and Dore Rivers in central France and the Meuse River in the Netherlands. Samples were collected from terraces formed during the last glacial cycle. Deposition age constraints were provided by ^{14}C dating, allowing for correction of post-depositional irradiation (Tebbens et al., 1999; Veldkamp and Kroonenberg, 1993). For the Allier and Dore Rivers, late Pleistocene to Holocene palaeo-erosion rates range from 40 to 70 mm/kyr, with the maximum value observed at the Pleistocene-Holocene transition (Figure 12). In the Meuse River, palaeo-erosion rates range from 30 to 80 mm/kyr showing a sharp decrease from the Late Pleistocene into the Holocene. This likely reflects a response of the fluvial system to external climatic forcing and possibly associated changes in vegetation cover.

McPhillips et al. (2013) reported cosmogenic nuclide-derived erosion rates from the Quebrada Veladera, a tributary of the Pisco River in the Western Andes (Peru). Late Pleistocene erosion rates were determined from 16 kyr-old terraces and Holocene rates from sediment in the active river channel, at different locations in the catchment (Figure 12). This spatial comparison between Pleistocene and Holocene rates showed that (i) small drainage areas are more sensitive to climate change, in this case a transition from wet to dry conditions at the end of the Pleistocene and (ii) the drainage network expanded upstream, *via* landscape dissection, during wet periods, while progressively annealing during dry periods.

In the same region, Bekaddour et al. (2014) investigated terrace sequences of the Pisco River. Episodes of sediment accumulation were correlated with pluvial periods 48-36 kyr (Minchin pluvial) and 26-15 kyr ago (Steffen et al., 2009). Cosmogenic nuclide-derived palaeo-erosion rates suggest a pulse of erosion during the Minchin pluvial period, with rates as high as 600 mm/kyr (Figure 12). This constrats with younger pluvial periods and present-day conditions which are characterised by little to no erosion. Bekaddour et al. (2014) proposed that these changes in erosion rates reflect shifts in the Inter Tropical Convergence Zone during the late Quaternary, which during the Michin period could have been located 100 km further south than it is presently. Furthermore, the pulse in erosion at this particular time is accounted for by the preceding poorly-erosive period, allowing the accumulation of regolith flushed during the Michin period.

Hidy et al. (2014) have used cosmogenic nuclide to quantify palaeo-erosion rates in alluvial deposits from Texas (USA) spanning over the past 500 kyr. These catchments were chosen because they are located in a tectonically quiescent region that has not undergone any glaciations, such that the role of climate on changes in erosion should be clearly identified. Erosion rates were found to be 30-35% higher during interglacial compared to glacial periods (Figure 12). For two rivers, erosion rates also correlated broadly with past temperatures, using $\delta^{18}O$ as a proxy. This correlation was interpreted as the role of warmer temperatures on promoting chemical weathering, which in turn enhances physical erosion. Observed increased erosion rates during interglacial periods are in agreement with predictions from the sediment flux model of Syvitski and Milliman (2007). The findings of Hidy et al. (2014) suggest that in catchments devoid of tectonic and glacial processes, climate has a direct role on erosion rates that can be accurately modelled. These observations imply lower erosion rates in the cool Quaternary compared to the warm Pliocene. This is at odds with globally-inferred higher erosion rates in the late Cenozoic (Herman et al., 2013; Métivier et al., 1999; Molnar, 2004; Zhang et al., 2001). The discrepancy was explained by Hidy et al. (2014) as these studies mainly focused on tectonically-active, glaciated regions, thus reflecting the dominant role of these fast eroding regions on global sediment fluxes (Milliman and Syvitski, 1992).

Quaternary Period:

Erosion products of the Quaternary period are deposited in different geologic settings (e.g. caves, alluvial sediment). Clastic material deposited in cave systems offer a unique setting to determine palaeo-erosion rates as no correction for post-depositional irradiation is needed. However, most cave studies have been interested in determining the sediment deposition age to determine fluvial incision rates as well as the age of hominid remains. Thus, the palaeo-erosion rates were only derived as a by-product.

In a study of caves from the New River valley (Virginia, USA; Granger et al., 1997), quartz vein clasts were amalgamated and analysed for ^{26}Al and ^{10}Be concentrations in order to determine sediment burial ages, inferred to range from 0.29 to 1.47 Myr. Palaeo-erosion rates were also derived from sand and amalgamated gravel samples ranging from 2 to 451 mm/kyr. A similar study was undertaken on sediment of Mammoth Cave to determine incision rates of the Green River (Kentucky, USA; Granger et al., 2001). Quartz gravel and sand were analysed to determine the age of cave formation. Slow palaeo-erosion rates ranging from 2 to 7 mm/kyr were derived from most of the past 3.5 Myr, with an increase to 30 mm/kyr in the Pleistocene.

Cyr and Granger (2008) compared erosion rates in the Apennines (Italy) derived from a range of techniques, including cosmogenic nuclides from cave sediment, to study variations in erosion rates over different timescales. They found similar values across timescales for the past 1 Myr, although all significantly lower than exhumation rates in the Pliocence. This was explained by hypothesizing that a state of dynamic landscape equilibrium may have been achieved over the past ~3 Myr.

In the southern Rocky Mountains (USA), Refsnider (2010) measured cosmogenic nuclide in cave sediment to infer a ten-fold increase in erosion rates from warm Pliocene conditions to a cooler Pleistocene (Thompson, 1991). This was interpreted to reflect the effectiveness of periglacial processes at high elevations.

Sediments deposited in alluvial settings have also been used to infer palaeo-erosion rates over the Quaternary Period (e.g. Balco and Stone, 2005; Charreau et al., 2011; Refsnider, 2010; Schaller et al., 2004; Schaller et al., 2002). Palaeo-erosion rates were derived from a 1.3 Myr-old terrace sequence of the Meuse River, in the Netherlands (Schaller et al., 2004). Constraints on the deposition age, required for post-depositional irradiation correction, were based on magnetostratigraphy of the sedimentary deposits (van den Berg and van Hoof, 2001). Calculated palaeo-erosion rates were uniform before 0.7 Myr ranging from 25 to 35 mm/kyr (Figure 13). After 0.7 Myr, they increased to reach a value of 80 mm/kyr in the late Pleistocene. This increase could be attributed to changing tectonic and/or climatic boundary conditions. The Ardennes Mountains and the nearby Rhenish massif were subjected to volcanic activity at around 0.65 Myr. This activity caused up to 250 m of uplift resulting in increased incision (e.g. Van Balen et al., 2000). However, at around the same time, the Middle Pleistocene transition occurred where the period of climatic cycles changed from 41 to 100 kyr and their amplitude increased (e.g. Mudelsee and Schulz, 1997). This change in period and amplitude might have influenced erosion with faster rates in the 100-kyr cycles compared to the 41-kyr cycles (e.g. Zhang et al., 2001).

In the Fisher Valley (Utah, USA), cosmogenic nuclides were measured in early and middle Pleistocene alluvial deposits (Balco and Stone, 2005). As terrace sediment was deposited subaerially and relatively slowly, the measured nuclide concentration was corrected for post-depositional irradiation. The depositional rate of the terrace material was inferred from dated ash layers and palaeo-soils. Palaeo-erosion rates determined from the inherited nuclide concentration varied between 80 and 220 mm/kyr. Modern rates determined from sediment of the active channel were ~125 mm/kyr. Balco and Stone (2005) observed no direct correlation of palaeo-erosion rates with climatic conditions. Instead, the results were interpreted as possibly reflecting episodic tectonically-induced subsidence of the sedimentary basin.

Palaeo-erosion rates have been determined from sediment of the northern Tianshan, spanning the past 9 Myr of erosion history of this region of central Asia (Charreau et al., 2011). Rates were inferred from cosmogenic nuclide measurements on sandstones from an intracontinental endorheic watershed, from late Pleistocene river terraces, and from the modern sediments of the Kuitun River. The measured nuclide concentrations in the sandstone sequence were corrected for post-depositional irradiation after sediment deposition and gradual burial of the deposits. Correction was also applied for post-depositional irradiation after Holocene incision of the Kuitun River into the sediment sequence. Palaeo-erosion rates were generally less than 1,000 mm/kyr for most of the past 9 Myr (Figure 13). However, between 2.5 and 1.7 Myr, erosion rates reached values as high as 2,500 mm/kyr interpreted as the response of catchment erosion to the onset of Quaternary glaciations at around 2 Myr. Nevertheless, the role of tectonics in this setting cannot be excluded and this will need to be addressed in future studies investigating changes in erosion rate at the million-year timescale.

Sediments delivered by the Nile River to the Mediterranean Sea is transported by longshore currents to the coastal plain of Israel. A suite of quartz sand samples was collected and analysed for ^{10}Be and ^{26}Al concentrations (Davis et al., 2012). Most samples were covered by a thick sedimentary overburden of tens of meters, therefore post-depositional irradiation was negligible.

Modern sand samples displayed a $^{26}Al/^{10}Be$ ratio of 4.8, lower than the expected production ratio of 6.8 and suggesting that they could have been buried at the study site for 600 to 700 kyr. Instead this was interpreted as the result of ^{10}Be and ^{26}Al decay during complex transport in the river system. This is easily understood as the Nile River is an extensive fluvial system where sediment transport from source to deposition areas is long and characterised by multiple episodes of temporary deposition and remobilisation. Furthermore, coastal plain sediment displayed constant ^{10}Be and ^{26}Al concentrations over the past 2.5 Myr. It was proposed that this illustrated the capacity of long and complex fluvial transport to homogenise multiple sediment sources and buffer the impact of climatic and/or tectonic variations on the cosmogenic nuclide budget of alluvial sediment at the million-year timescale.

4 Discussion

In this section, we assess how results from uranium and cosmogenic nuclide studies contribute to understanding the links between climate and fluvial dynamics in the context of previous works (Table 6). Because of the challenge to quantify tectonic processes over timescales shorter than a million years, climate is often considered as the major driver of erosion changes when focusing on the late Quaternary. However, where the period of time considered reaches as far back as 9 Myr, the role of tectonics cannot be ignored. In central Asia, Charreau et al. (2011) attributed the increase in erosion rates at around 2 Myr to the onset of glaciations. Nevertheless, this could also be explained by a pulse in uplift.

In Western Europe, differentiating between climatic or tectonic drivers is equally challenging. The increase in cosmogenic nuclide-derived erosion rates at ~0.7 Myr in the Meuse River could be attributed to uplift in the Ardennes Mountains or to the change in period of climatic cycles from 41 to 100 kyr. In contrast, in the Fisher Valley (Utah, USA) Balco and Stone (2005) saw no clear imprint of climatic cycles in catchment erosion. Instead, they attributed changes in erosion rates to increased basin subsidence. In the Nile River, Davis et al. (2012) did not observe any changes in cosmogenic nuclide-derived erosion rates over the past 2.5 Myr. This was explained by the capacity of large river systems to buffer erosion variability, not only over spatial scales but also temporal scales.

In summary, at the million-year timescale it is difficult to assess the role of climate variability on catchment erosion because it can be partially or completely overprinted by tectonic processes.

At the Holocene/Late Pleistocene timescales, some studies of palaeo-erosion rates suggest faster erosion rates during cold periods (Fuller et al., 2009; Schaller et al., 2002) while others propose the opposite (Bekaddour et al., 2014; McPhillips et al., 2013). Fuller et al. (2009) interpreted faster rates during the LGM as the response to higher rainfall in the response to higher rainfall in the Sierra Nevada (USA) during that period of time. This is surprising since the LGM is generally described as drier than the Holocene. Observations of a wet LGM in this region were derived from pollen data (Adam and West, 1983). Precipitation estimates may not be accurate as the transfer function used between pollen record and precipitation may be influenced by elevation (rain shadow effect) instead of actual effective rainfall changes. Thus, it is more likely that fast erosion rates during the LGM would be explained by the effectiveness of periglacial processes as physical weathering agents (Dühnforth et al., 2010; Small et al., 1999). The effect of frost-driven sediment production on erosion is illustrated by the study of Marshall et al. (2015) in the Oregon Coast Range (USA) where they showed that erosion rates were 2.5 times faster during the LGM compared to present. Similarly, Schaller et al. (2002) attributed the faster cosmogenic nuclide-derived and modelled erosion rates during the LGM as a result of periglacial processes in Europe while in the Holocene interglacial conditions promoted vegetation development and increased soil cover preservation. The importance of periglacial processes was also noted at the million-year time scale in the southern Rocky Mountains (USA), as it was proposed they have driven a ten-fold increase in erosion rates during the Pleistocene (Refsnider, 2010). In contrast, in southern USA, Hidy et al. (2014) observed increased erosion during interglacials in catchments devoid of tectonic activity and located far away from the influence of glaciers even during the LGM. This could suggest that at the 10-kyr timescale, the response of catchment erosion to climatic variability depends on whether periglacial processes were operating during cold periods: in regions where they were, erosion was more active during cold periods; in other areas, erosion was enhanced during warmer periods.

Faster erosion rates during the LGM, as suggested by Schaller et al. (2002) and Fuller et al. (2009), are at odds with studies pointing toward lower rates during glacial periods (Bookhagen et al., 2006; Bookhagen and Strecker, 2012; Bookhagen et al., 2005b; Clift et al., 2008; Hu et al., 2012; Trauth et al., 2000; Trauth et al., 2003; Uba et al., 2007), including using cosmogenic nuclide-derived palaeo-erosion rates (Bekaddour et al., 2014; McPhillips et al., 2013). In these studies, faster erosion rates during wet periods have been inferred for the Himalaya and the Andes. This contrasts with the old, slowly eroding Massif Central studied in Schaller et al. (2002). However, Fuller et al. (2009) focused on the Sierra Nevada (USA) which uplifts at a rate comparable to the Andes. Nevertheless, erosion rates in the Andes are faster and mass wasting more frequent than in the Sierra Nevada (Blodgett and Isacks, 2007; Riebe et al., 2000). Thus, the occurrence of mass wasting and the magnitude of erosion rates may dictate how catchment erosion responds to climatic cycles at the 10-kyr timescale. Despite periglacial processes being efficient agents of erosion in the Himalaya and Andes during glacial periods, the increase in mass wasting during wet periods could be the main driver for change in erosion (e.g. Bookhagen et al., 2005b). The role of vegetation cover may also amplify this relationship: Istanbulluoglu and Bras (2005) showed that under denser vegetation cover (likely during warm periods), landscapes may become landslide-dominated. However, Carretier et al. (2013) presented an inverse correlation between erosion rates and the density of vegetation cover, suggesting faster erosion of sparsely-vegetated landscapes during cold periods.

Another aspect that may account for differences between cosmogenic nuclide studies and other types of work is the size of the drainage area integrated. The cosmogenic nuclide-derived erosion rates reflect conditions in the sediment source area of the catchment. In contrast, Clift et al. (2008a) and Uba et al. (2007) studied changes in erosion for Asian rivers by investigating delta or marine sediment. If alluvial plains act to buffer the headwater fluvial response to climate variability, it is expected that this response will be different whether focusing on the sediment source region or including the alluvial plain. Sediment storage in alluvial plains can induce a time lag between the upstream fluvial response to external perturbations and its manifestation in estuaries/deltas or oceanic basins, resulting in a decoupling between the fluvial response in source and sink regions. For instance, uranium-series isotope studies of large river systems showed that it can take from a few to several 100 kyr for sediment to be transported from source to sink regions (Chabaux et al., 2012; Dosseto et al., 2006b; Granet et al., 2010; Granet et al., 2007). For these reasons, caution must be taken when inferring links between erosion and climatic variability (or tectonic, or anthropic) from sedimentary deposits in oceanic basins, or simply far from sediment source regions. It is possible to reconcile cosmogenic nuclide studies and other type of works when acknowledging the time lag to transport "information" (i.e. fluvial response) from sediment source regions to depositional environments.

The few available studies that have applied comminution dating to sedimentary deposits suggest that:

1. The residence time of sediment in catchments follows glacial-interglacial periods, illustrating that fluvial dynamics is in sync with climatic cycles (at least at the 10-kyr to 100-kyr timescale);
2. Variations in residence time reflect changes in sediment provenance. This implies that climate variability not only drives changes in erosion rates but also dictates what sediment stores are tapped by erosion.

DePaolo et al. (2006) showed that in the north Atlantic, erosion of exposed European continental shelves was promoted, accounting for observed long regolith residence times during glacial periods. In southeastern Australia, the contrast in regolith regolith residence time between glacial and interglacial periods was not as marked as in the northern Atlantic. During interglacial periods, longer residence times were interpreted as the result of the mobilisation of alluvial deposits and/or old colluviums while the upper catchment delivered little sediment to the main channel. Vegetation cover was invoked as an important link between climate and catchment erosion, governing the origin of sediment (Dosseto et al., 2010). These results support the thesis that during warm periods, increased vegetation cover tends to inhibit erosion (Burbank et al., 1993; Langbein and Schumm, 1958). More active erosion in the sediment source region during the LGM is consistent with observations in other regions where periglacial processes have occurred while mass wasting is marginal (Fuller et al., 2009; Schaller et al., 2002).

5 Conclusions and perspectives

When compared to the in-situ cosmogenic nuclide technique, which has benefited of decades of investigations and improvements, the application of uranium-series isotopes to landscape evolution problems is still in its infancy. Although uranium-series isotopes have been studied since the 1960's, the complexity of the occurrence of radioactive disequilibrium in weathering products has hindered their application for a long time. It is only over the past ten years that there has been a rejuvenation of this technique, triggered by analytical advances in mass spectrometry. This is illustrated by the emergence of new approaches such as the comminution dating technique.

The use of cosmogenic nuclides to determine catchment-wide erosion rates is widely used and accepted. The application to sedimentary archives offers a unique tool to determine erosion rates over the last few million years (e.g. Charreau et al., 2011) or the last glacial cycle (e.g., Fuller et al., 2009). Studies where cosmogenic nuclide-derived palaeo-erosion rates are determined over the last glacial cycle illustrate that the actual change in erosion rate is damped and delayed because a time lag exists between a change in erosion rates and when it is actually recorded by cosmogenic nuclide.

An exciting perspective is the combination of comminution age with cosmogenic nuclide. One assumption of the cosmogenic nuclide technique to determine erosion rates is that the transport time in the river system is short relative to the erosional timescale. While this is reasonable for many small catchments, it is less likely to be true for large ones. Knowing the comminution age (U-series) or floodplain sediment storage time (in situ-produced ^{14}C) would help to correct for the cosmogenic nuclide produced during transport of the sediment in the river system. Unfortunately, the techniques of comminution age and cosmogenic nuclide make use of different grain size fractions (<50 μm for the former, generally >125 μm for the latter). This means that the comminution age may not be directly applicable to correct for the transport time of the coarser quartz fraction. A promising new technique based on the measurement of the

^{10}Be(meteoric)/^{9}Be ratios opens the possibility to determine erosion as well as weathering rates from fine-grained river sediment (Bacon et al., 2012; Nichols et al., 2014; Reusser and Bierman, 2010; von Blanckenburg et al., 2012; West et al., 2013; Wittmann et al., 2012). The grain size fraction generally used in this technique (30-40 μm) is comparable with that used in the comminution age determination.

From the volume of work produced so far, we can summarise the contribution of cosmogenic nuclide and U isotopes to the study of the catchment erosion response to climate change, as follows:

1. At the 10-kyr to 100-kyr scale, regolith residence time is in sync with climatic cycles. This reflects changes in the source of sediment. At the catchment scale, the role of climate on vegetation cover is believed to be the main driver of the switch between sediment sources. At a larger scale (e.g. North Atlantic), it is clearly seen in the sedimentary record that sediment delivered to oceanic basins may undergo storage on continental shelves for long periods of time, depending on sea level fluctuations;
2. Periglacial processes have a major role on how catchment erosion responds to climatic variability at the 10-kyr scale. In their absence, erosion is faster during warm periods; while where they occur, the response varies;
3. In settings where periglacial processes occur, mass wasting and the magnitude of erosion rates dictate the relationship between climate and erosion. In fast eroding terrains where mass wasting dominates (e.g. Himalaya, Andes), erosion is faster during warm periods; while it is slower in regions characterised by more moderate erosion rates and marginal mass wasting.

In the future, U-series and cosmogenic nuclide should be combined with other tools and approaches to specifically test the relationships described above. This will lead to an improving understanding of how natural systems operate, and will also assist in how to better plan for the future in a changing environment.

Acknowlegements

We would like to thank Kyungsoo Yoo, Heather Handley, Ashley Martin, Victoria Lee and Ken Ferrier for helpful discussions. We also thank Amy Dougherty for her comments on this manuscript. This work was funded by an Australian Research Council *Future Fellowship* FT0990447 to AD.

Figures caption

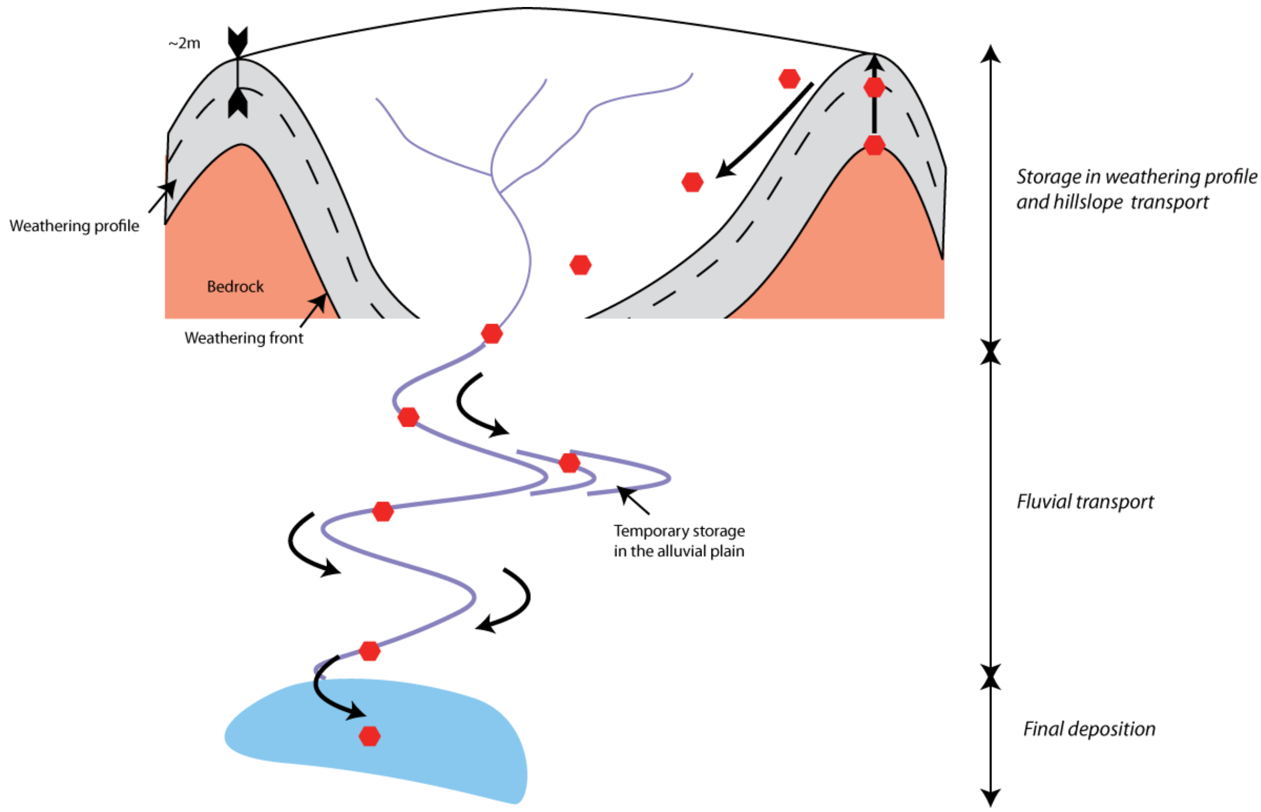

Figure 1. Conceptual representation of regolith transit from source to sink. Regolith (polygons) “enters” the catchment at the weathering front. At that moment, the U isotope clock starts “ticking”. *In situ*-produced cosmogenic nuclides start accumulating in the regolith only when erosion brings them within ~2-3m of Earth’s surface. Thus, if the weathering profile is thicker than 2m, the U isotope clock starts ticking before the cosmogenic nuclide clock. The *regolith residence time* in the catchment, as inferred by uranium isotopes, amounts to the sum of storage in weathering profiles, hillslope and fluvial transport. Cosmogenic nuclides accumulate continuously in regolith during erosion within the top 2-3m of the weathering profile and the hillslope. Then, during fluvial transport and final deposition, cosmogenic nuclide concentrations will decrease or increase depending on the cosmogenic nuclide, the storage depth and duration.

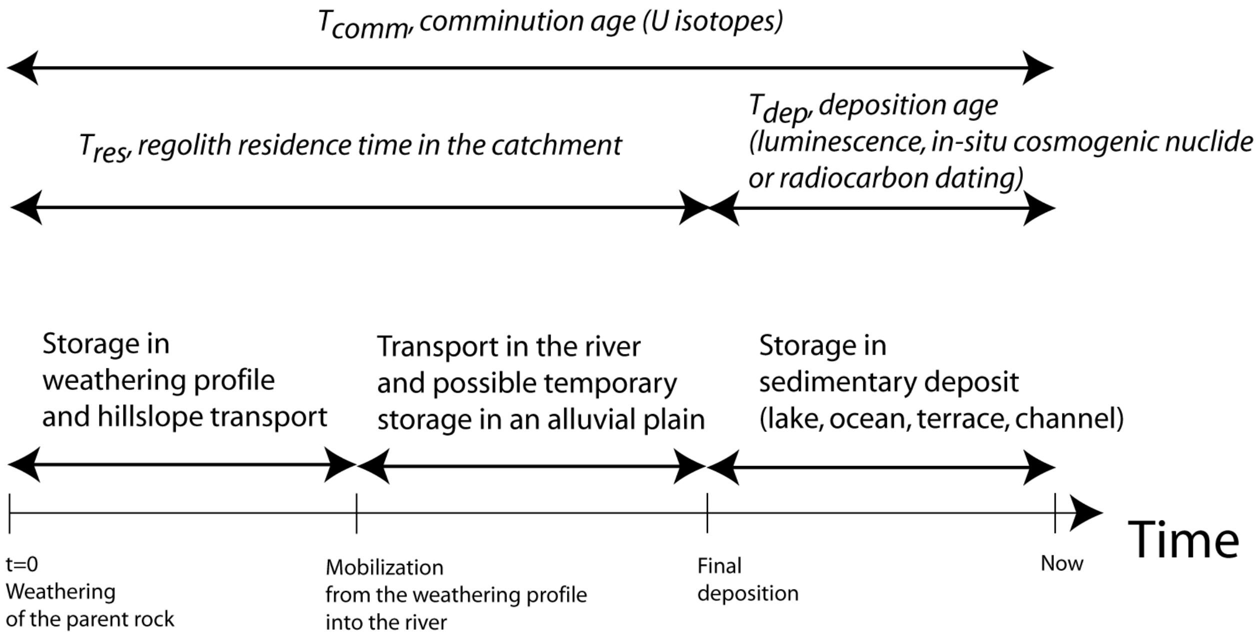

Figure 2. Conceptual representation of the comminution age and the regolith residence time (modified from Dosseto et al., 2010a).

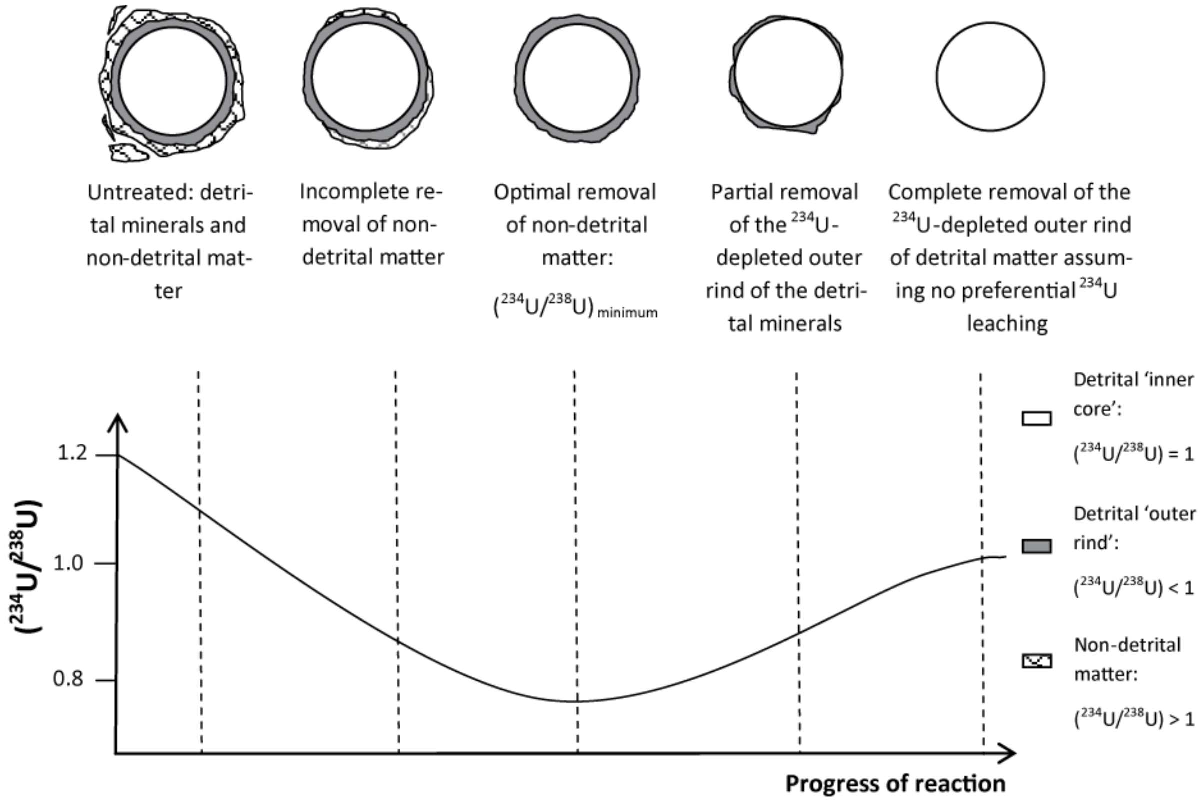

Figure 3. Approach for evaluating the adequacy of sample leaching (Lee, 2009; Martin et al., 2015). The optimum sample leaching protocol should result in the lowest $(^{234}U/^{238}U)$ ratio in the leached residue. Because solution-derived and organic phases have $(^{234}U/^{238}U) >1$, a protocol where the removal of these phases is incomplete will result in a $(^{234}U/^{238}U)$ ratio higher than with the optimum protocol. In contrast, if the protocol is too aggressive and attacks the surface of rock-derived minerals, the rind that contains the ^{234}U depletion will be partially or completely removed, resulting in a $(^{234}U/^{238}U)$ ratio in the leached residue higher than if the surface were intract. Modified from (Martin et al., 2015).

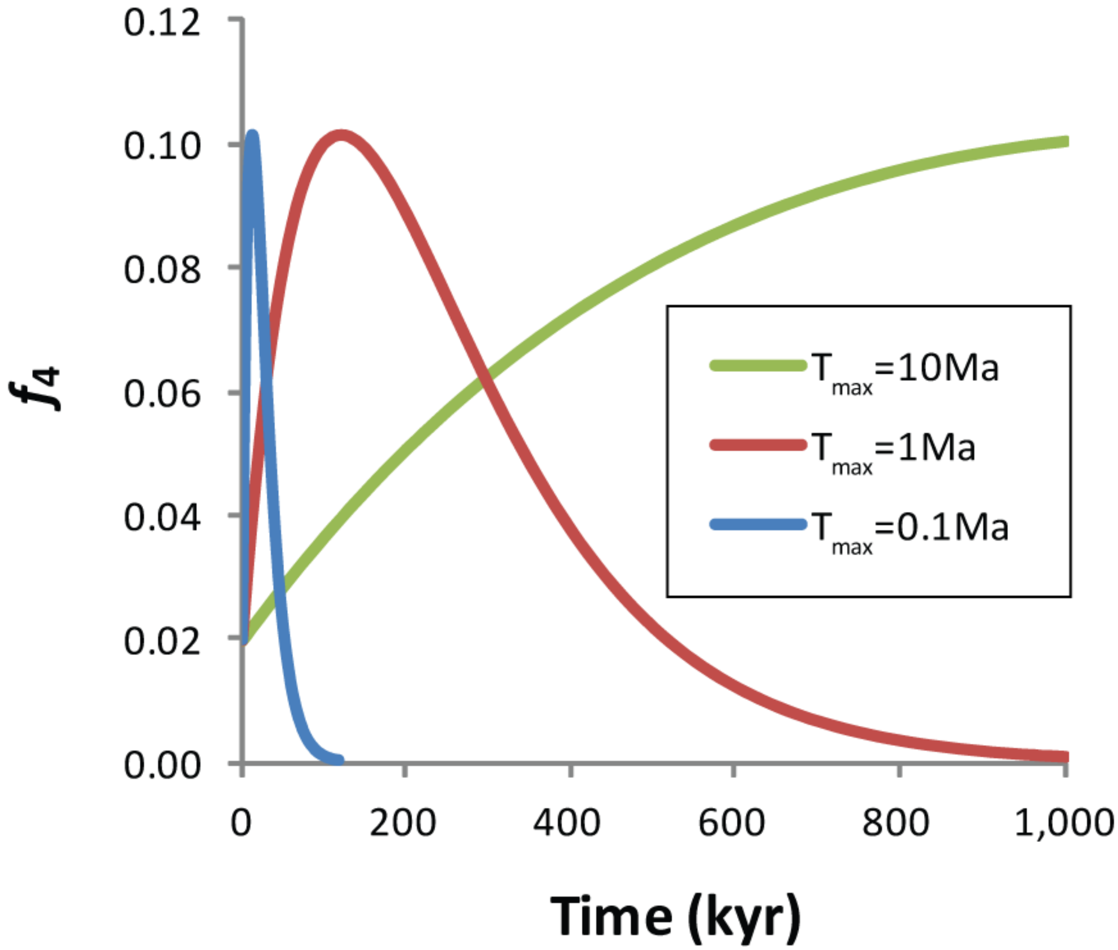

Figure 4. Modelled variation of the recoil loss fraction, f_4, with time for different values of T_{max}, the amount of time required to create a particle of maximum roughness. See text for details.

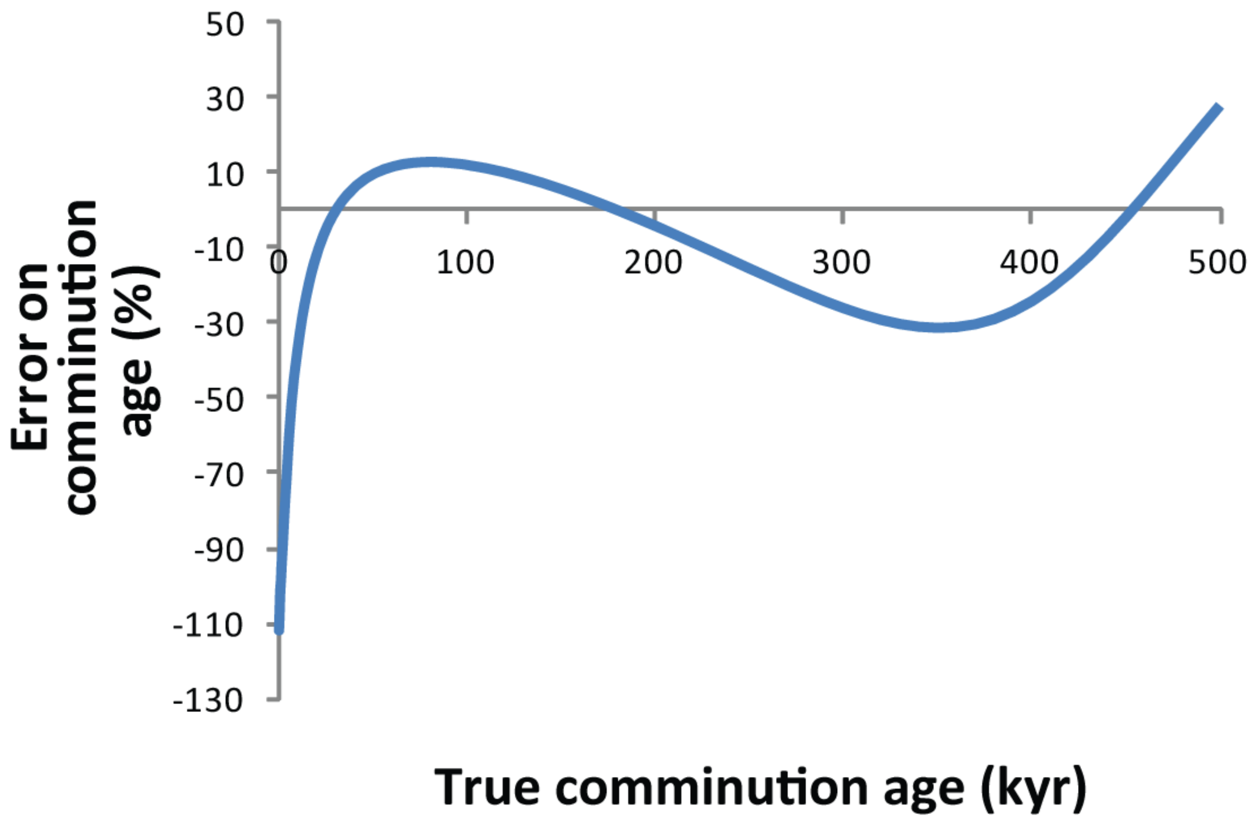

Figure 5. Difference between calculated comminution ages considering a time-dependent f_4 and a constant f_4, as a function of the true comminution age. See text for details.

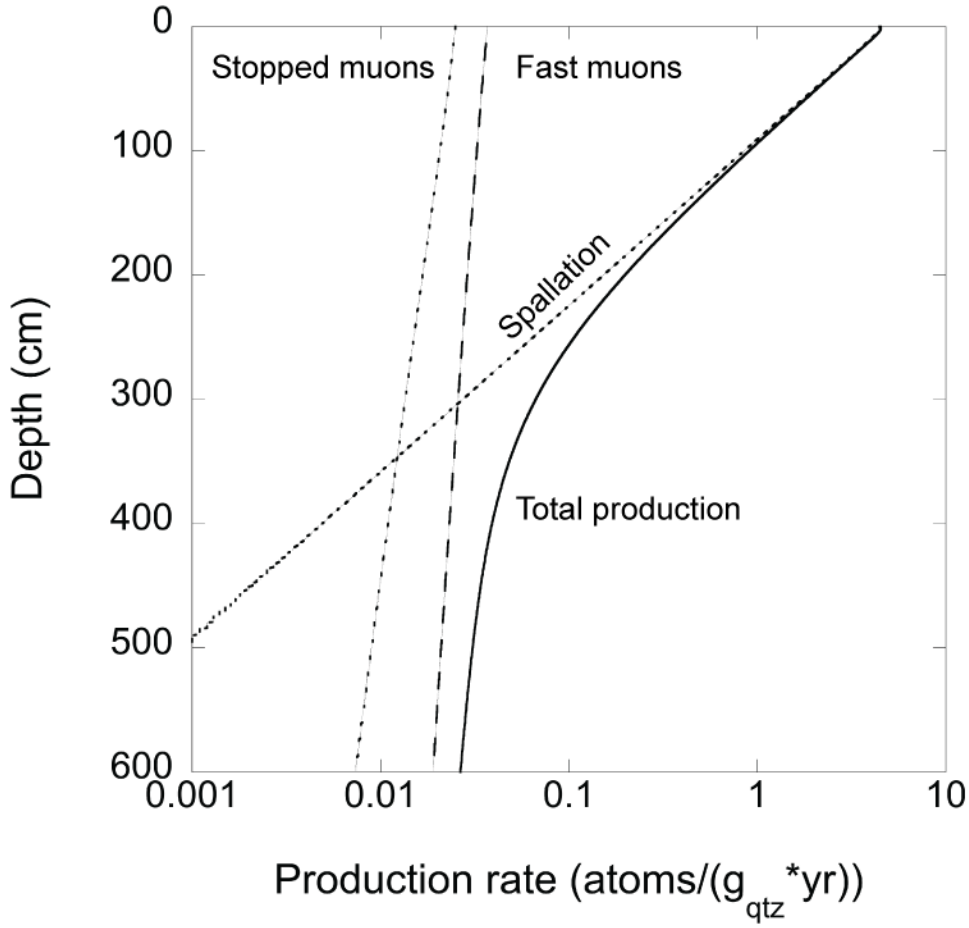

Figure 6. Production rate of *in situ*-produced cosmogenic ^{10}Be as a function of depth, at sea-level and high latitude. The total production is a composite of production by spallation (nucleons such as protons and neutrons), fast and stopped muons. Production in rock is dominated by muons at depth greater than 300 cm.

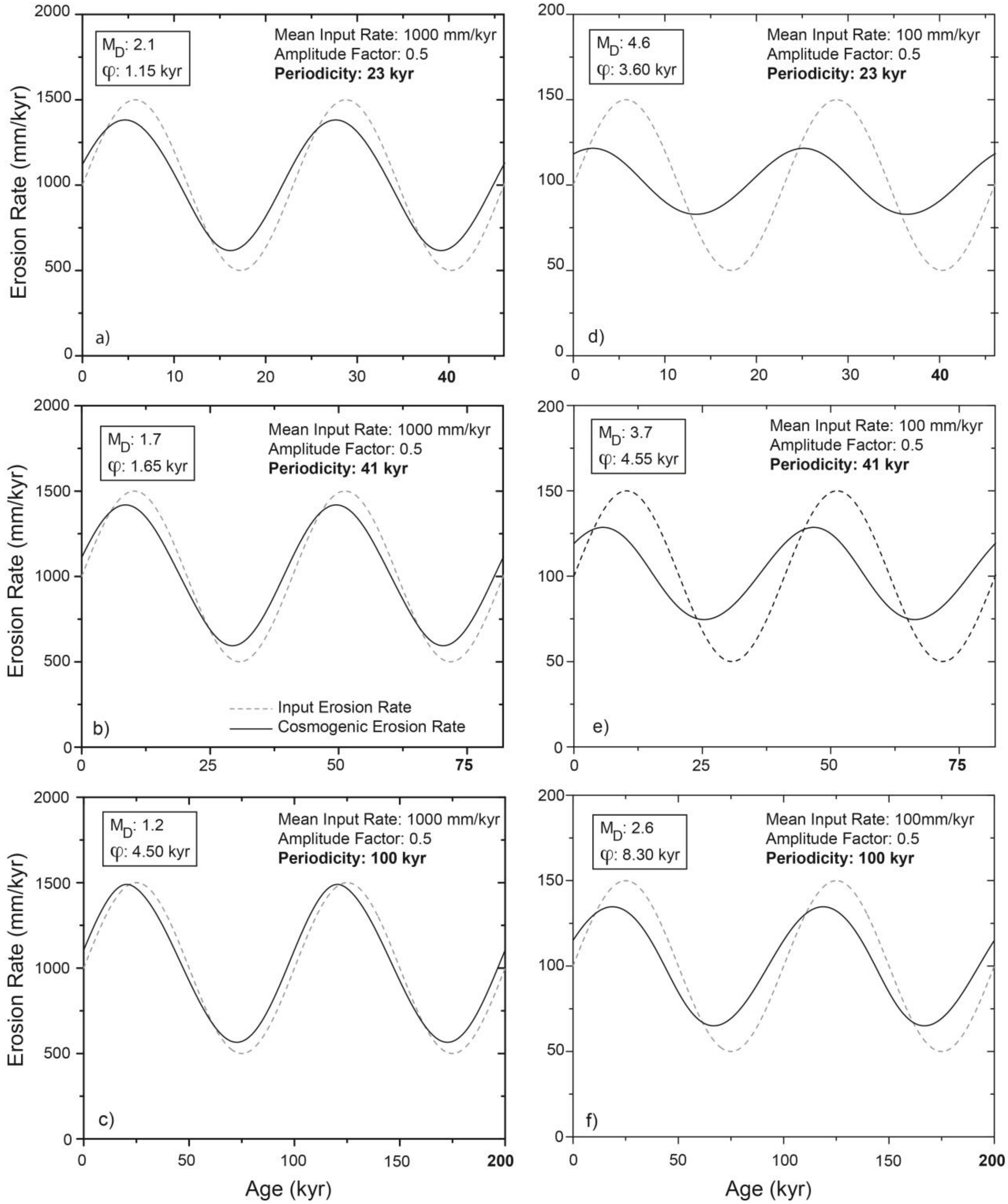

Figure 7. Models illustrating how cosmogenic nuclide-derived erosion rates (solid curves) record modelled input (true) erosion rates (dashed curves). Cosmogenic nuclide-derived erosion rates lag behind the input erosion rate and may not equilibrate with it. Depending on the periodicity, amplitude factor (0-1) of the erosion rate and mean input erosion rate, the cosmogenic nuclide-

derived rate lags more or less behind the input erosion rate. This lag-time φ is reflected in the phase-lag (in kyr) of the maximum cosmogenic nuclide-derived to the input erosion rate. For instance, three different periodicities (23, 41, and 100 kyr) are shown for two different mean input erosion rates (1,000 mm/kyr (a–c) and 100 mm/yr (d–f)), but constant amplitude factor (0.5). The phase-lag φ increases with longer periodicity (a–c or d–f) or decreasing mean input erosion rates (e.g. a and d). Taken from Schaller and Ehlers (2006).

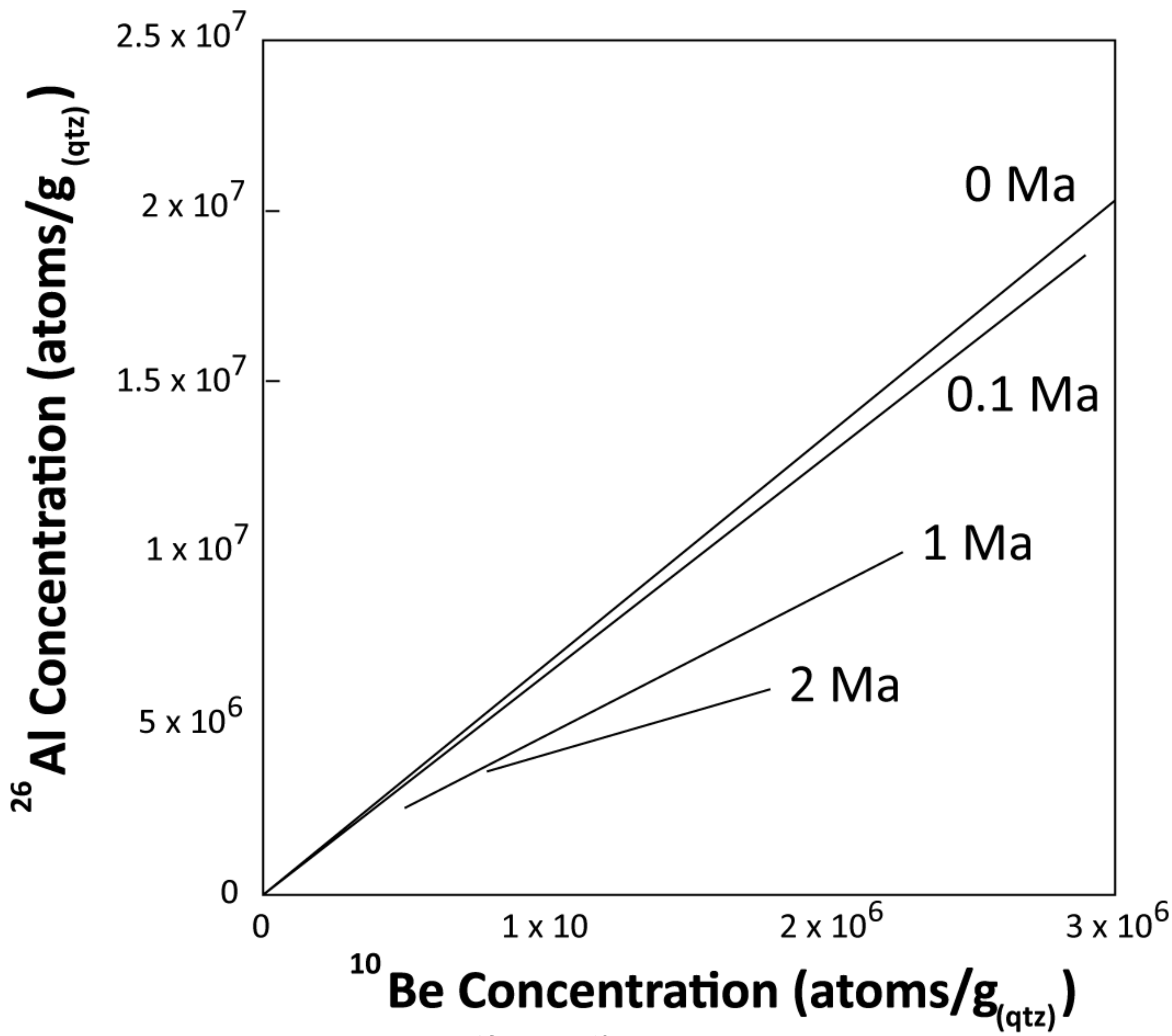

Figure 8. Isochron burial diagram for ^{26}Al and ^{10}Be used to derive deposition ages (Balco and Rovey, 2008). For instance, several clasts are collected at the same depth of the sediment deposit, but contain different inherited nuclide concentrations. The concentrations of the clasts at the time of deposition form a line (*isochron*) in this diagram whose slope is defined by the production ratio of the two cosmogenic nuclides. Following decay and possible post-depositional irradiation, the slope of the isochron decreases with increasing time since deposition. The slope of the isochron can then be used to determine the burial age of the clast layer.

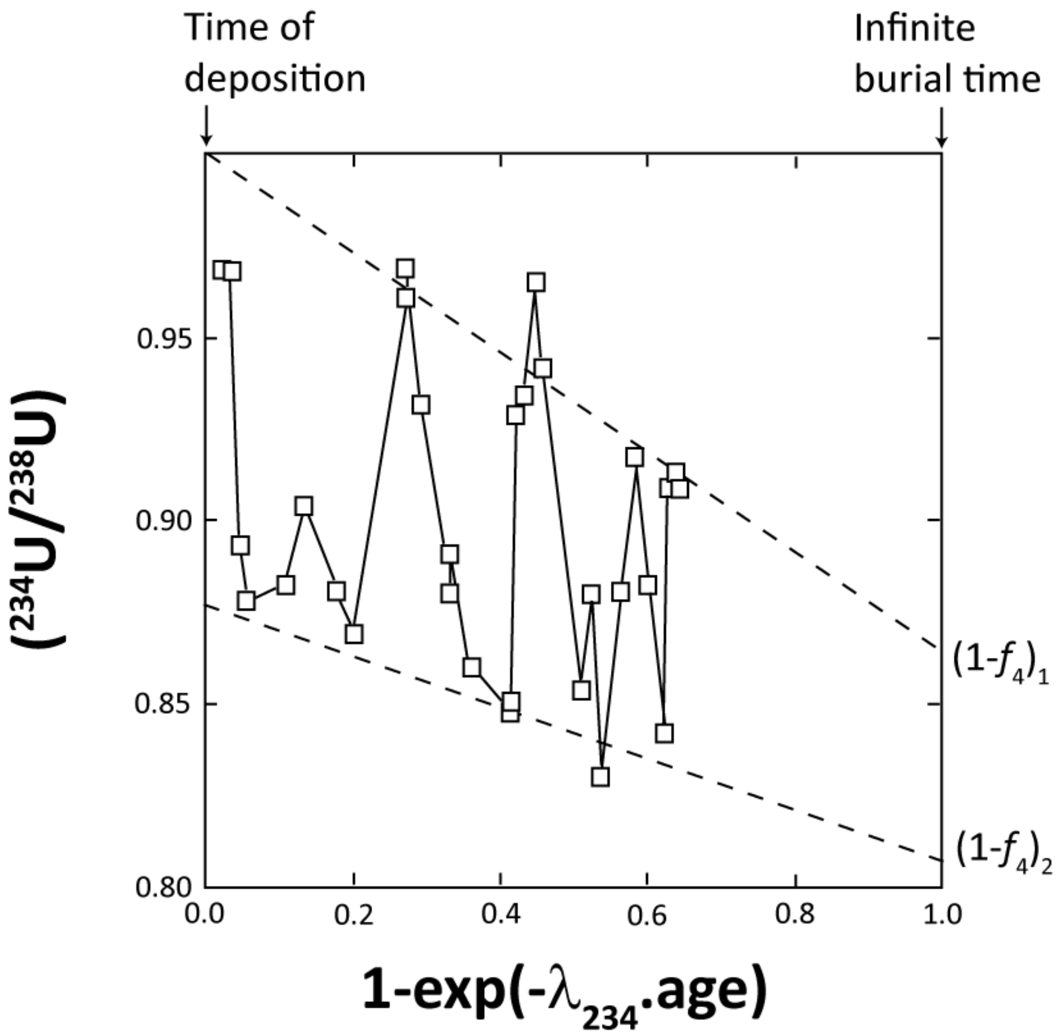

Figure 9. $(^{234}U/^{238}U)$ activity ratio in deep-sea sediment from ODP Site 984A as a function of their deposition age (DePaolo et al. 2006). Two sediment populations were identified, reflecting distinct sediment sources: Iceland (with a high $(^{234}U/^{238}U)$, ε_{Nd} and low $^{87}Sr/^{86}Sr$) and continental Europe (with a low $(^{234}U/^{238}U)$, ε_{Nd} and high $^{87}Sr/^{86}Sr$). Two values for the recoil loss fraction, f_4 (termed f_α in DePaolo et al. 2006), were determined graphically from the intercept of the dashed lines with $1-e^{-\lambda_4 t}=1$ which is equal to $(1 - f_4)$. The upper dashed line corresponds to the Iceland sediment end-member (f_4 = 0.135), while the lower dashed line corresponds to the continental Europe sediment end-member (f_4 = 0.19). Modified from (DePaolo et al. 2006).

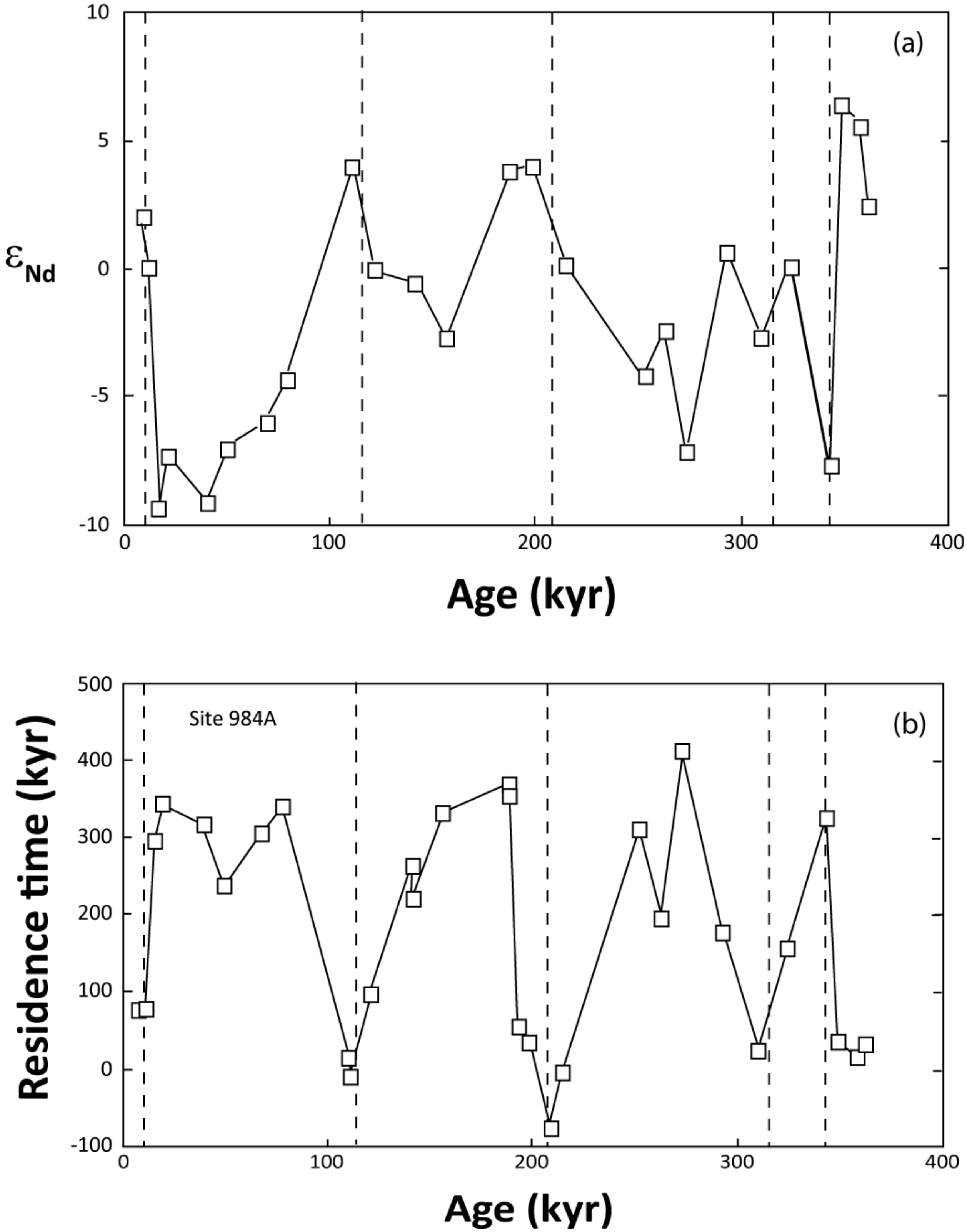

Figure 10. (a) Nd isotope ratios and (b) calculated regolith residence times in deep-sea sediment from ODP Site 984A (DePaolo et al. 2006). Nd isotope compositions reflect variations in contribution from sediment derived from Iceland (high ε_{Nd}) and continental Europe (low ε_{Nd}).

Regolith residence times also reflect these changes in sediment source: during interglacials, sediment was mostly derived from Iceland and characterised by a short residence time (i.e. rapid delivery to the depositional environment), while during glacial periods Iceland being covered by a thick ice sheet, sediment was mostly derived from continental Europe and characterised by long residence times (probably reflecting storage on continental shelves exposed and eroded during glacial periods). Modified from DePaolo et al. (2006).

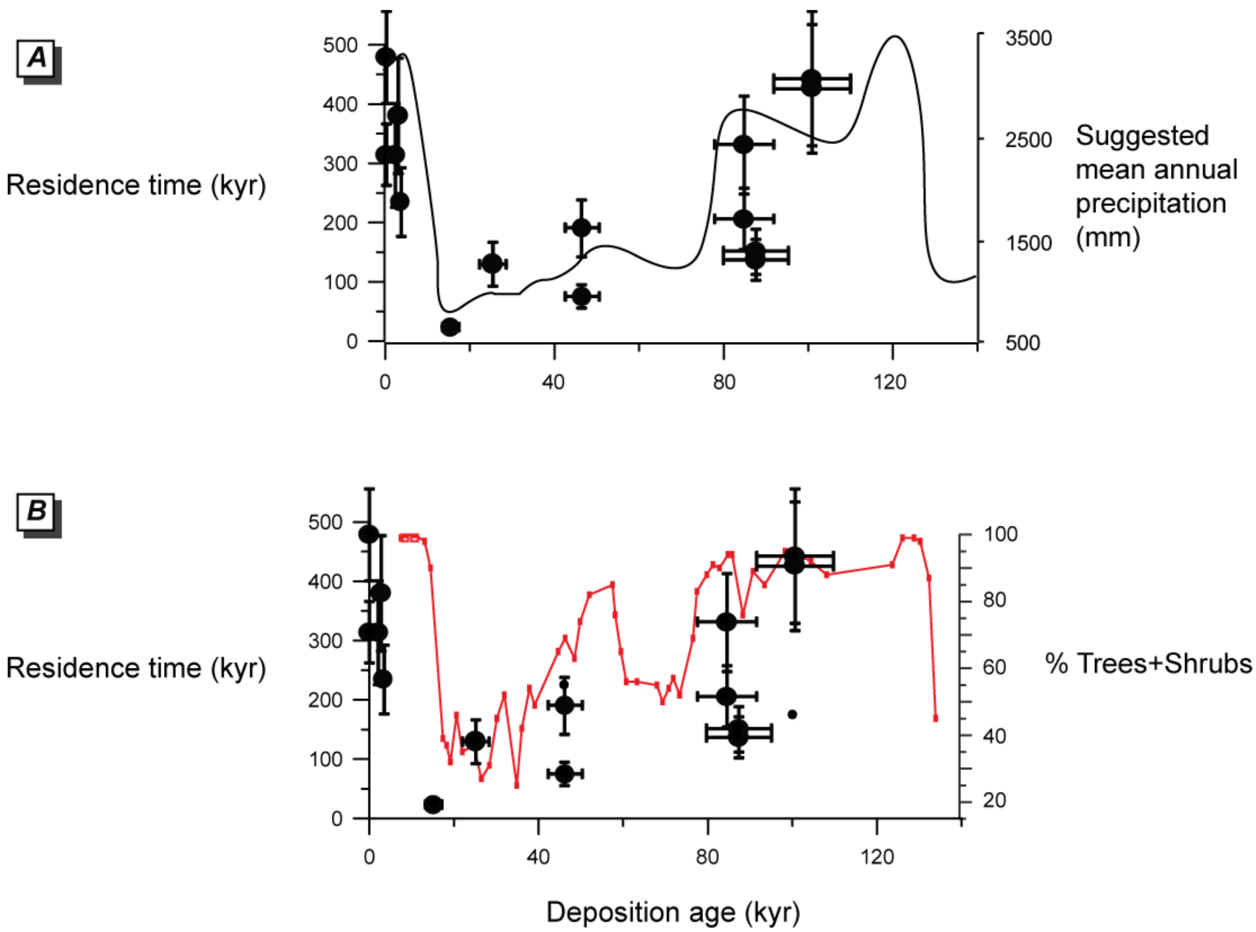

Figure 11. Variations of the regolith residence time in the Murrumbidgee catchment as a function of the deposition age. The residence time is compared to (a) suggested mean annual precipitation (in mm) (Kershaw, 1986) and (b) percentage of trees and shrubs in pollen data from DSDP site 594 (Barrows et al., 2007; Heusser and van de Geer, 1994). Uncertainties on the residence time are given at the 2σ level. A high percentage of trees+shrubs indicates that the upper catchment was mostly covered by trees, whereas a low percentage suggests that shrubs were mostly present. Modified from Dosseto et al. (2010).

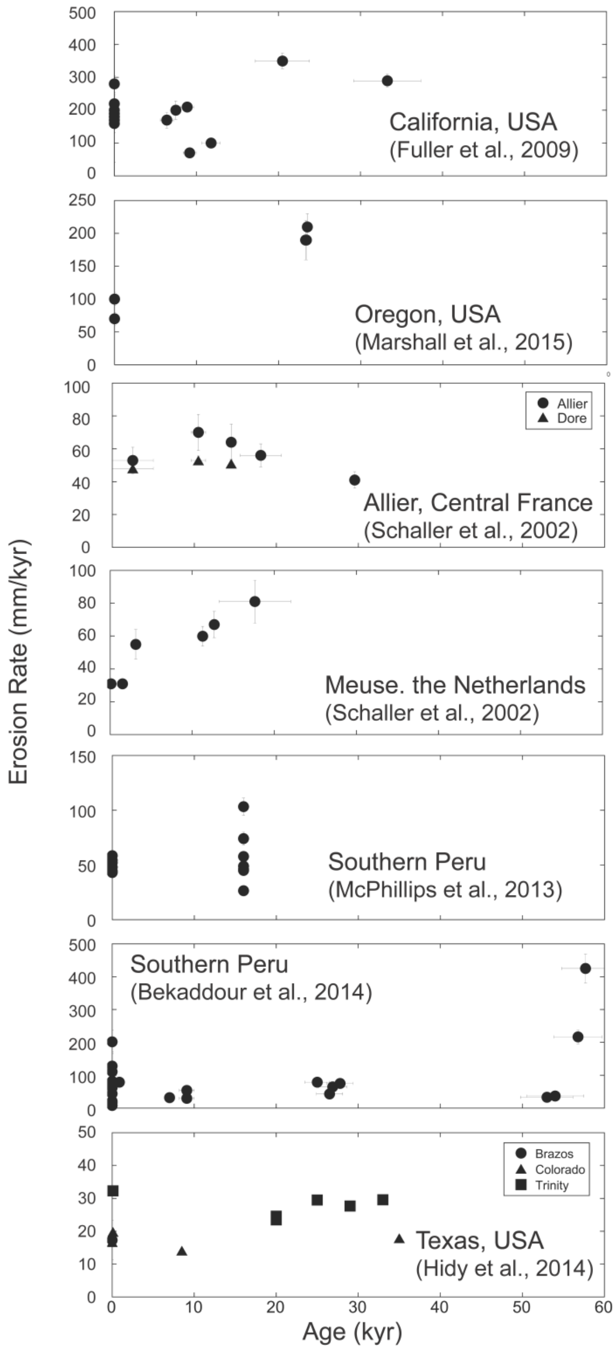

Figure 12. Late Pleistocene to Holocene cosmogenic nuclide-derived erosion rates from seven sites that span over the last 30 to 60 kyr. Study areas range from California (Fuller et al., 2009) and Oregon (Marshall et al., 2015) in the Western USA, Southern Peru (McPhillips et al., 2013; Bekaddour et al., 2014), Central Europe (Schaller et al., 2002) to Texas, USA (Hidy et al., 2014). Erosion rates are plotted as reported by the authors. No re-calculation was done for consistent production rates and half-lives.

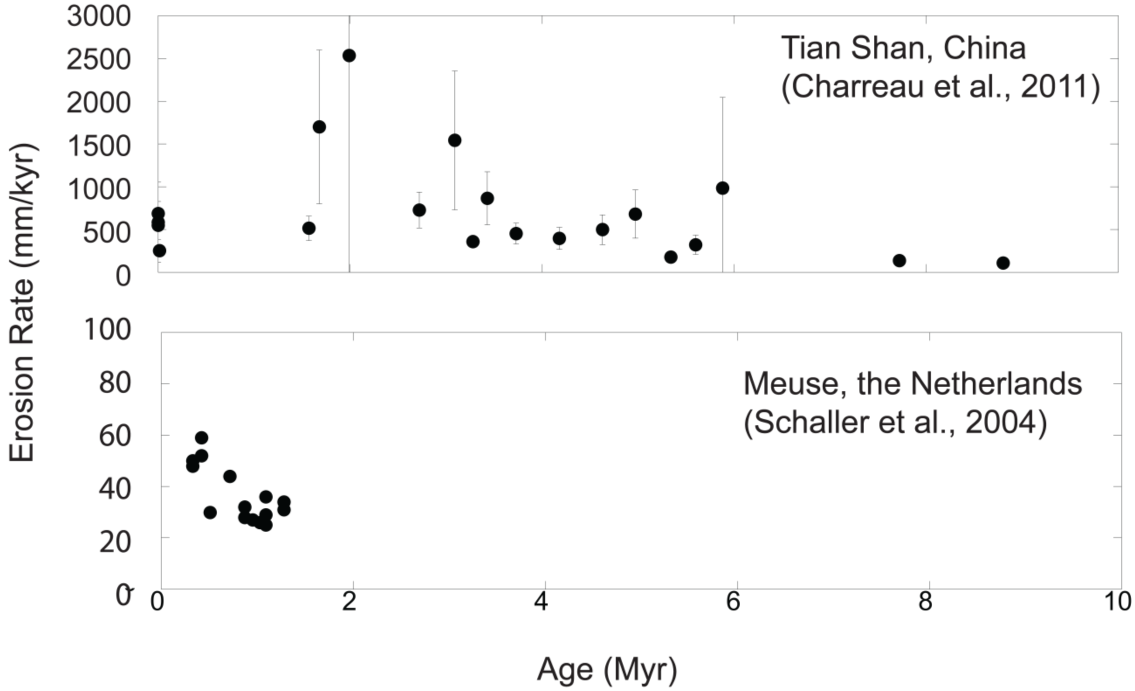

Figure 13. Cosmogenic nuclide-derived erosion rates from two locations spanning over more than a million years. In the Tian Shan (Charreau et al., 2011) increased rates at 2 million years are attributed to onset of glaciation. The observed increase in erosion rates of the Meuse river (Schaller et al., 2004) could be caused by the Middle Pleistocene transition. However, in both cases the influence of tectonic changes on erosion rates cannot be excluded.

Tables

Table 1. Glossary of terms used

Term	**Definition (as used by the authors)**
Erosion	This process involves transport of material, whether it is physical erosion (sediment transport) or chemical erosion (solute transport).
Weathering	Transformation of the parent rock to smaller constituent blocks either by physical (e.g. frost shattering, root action) or chemical weathering (e.g mineral dissolution).
Regolith	The solid product of erosion, i.e. the residue of physical and chemical weathering of the parent rock. The term regolith includes saprolite and soil.
Saprolite	The solid residue of physical and chemical weathering of the parent rock; it is immobile (i.e. no colluvial transport) and generally preserves some physical structure of the parent rock.
Soil	The solid residue of physical and chemical weathering of the parent rock. It is mobile (i.e. can be transported from the weathering profile) and is produced from the saprolite or directly from the parent rock.
Comminution age	The amount of time elapsed since a material acquired its final size and surface properties. When applied to erosion products, it is assumed to represent the amount of time since production of fine-grained regolith from the parent rock.
Regolith residence time	The residence time of regolith in a catchment (before final deposition in a fluvial terrace, palaeo-channel, lake or ocean). This time tracks the travel of regolith from source to sink and encompasses (i) storage in weathering profile, (ii) hillslope transport, (iii) fluvial transport and (iv) possible temporary storage in an alluvial plain. Note the term "*transport time*" is used in DePaolo et al. (2006) and Lee et al. (2010) instead of *residence time*. However, the term "*transport time*" can be easily confused with the time of fluvial transport, which is only a fraction of the residence time.

Table 2. Parameters used for U-series isotope models

Parameter	**Description**	**Units**
N_8, N_4	Concentrations of ^{238}U and ^{234}U, respectively	atoms.g^{-1}
λ_8, λ_4	Decay constants for ^{238}U and ^{234}U, respectively	yr^{-1}
w_8, w_4	Dissolution coefficients for ^{238}U and ^{234}U, respectively	yr^{-1}
Γ_8, Γ_4	Gain coefficients for ^{238}U and ^{234}U, respectively	yr^{-1}
f_4	Fraction of recoiled ^{234}Th (and thus ^{234}U)	unitless
t_{comm}	Comminution age	yr
τ_{recoil}	Timescale of ^{234}U depletion by recoil	yr
$\tau_{dissolution}$	Timescale for removing a layer of thickness equivalent to the ^{234}Th recoil length by dissolution	yr
R	Mineral dissolution rate	mol.m^{-2}.yr^{-1}
M	Mineral molar mass	g.mol^{-1}
U	Uranium concentration	g.g^{-1}
L	Recoil length	m
r	Mineral grain radius	m
λ_r or λ_s	Surface roughness	unitless
K	Grain shape factor	unitless (=6 for a sphere)
β	Mineral grain aspect ratio	unitless
$X_{\overline{d_p}}$	Mass or volume fraction of sediment over a given grain size interval	unitless
$\overline{d_p}$	Mean particle diameter for a given grain size interval	m
S or A	Specific surface area	m^2.g^{-1}
ρ	Density	g.m^{-3}
a	Size of the adsorbate molecule used for surface area measurement	m
D	Fractal dimension of the sediment surface	unitless

Table 3. Protocol for sequential leaching of soil and sediment samples (Martin et al., 2015)

Leached fraction	**Reagents**	**Process**
Carbonates	16 mL of sodium acetate adjusted to pH 5 with acetic acid + 30 mg of sodium citrate	Agitate at room temperature for >5 hours.
Fe-Mn oxides	40 mL of hydroxylamine hydrochloride in 25% (v/v) acetic acid + 30 mg of sodium citrate	Heat at 95°C for 6 hours, occasionally agitating.
Organics – step 1	6 mL 0.02M nitric acid + 10 mL 30% hydrogen peroxide, adjusted to pH 2 with nitric acid + 30 mg of sodium citrate	Allow organic matter to react with hydrogen peroxide solution at room temperature for 5-20 min (longer for higher organic content), then warm slowly until bubbling from the strongly exothermic reaction diminishes (total of 30 min). Heat at 85°C for 1.5 hours, occasionally agitating.
Organics – step 2	6 mL 30% hydrogen peroxide, adjusted to pH 2 with nitric acid + 30 mg of sodium citrate	Heat at 85°C for 3 hours, occasionally agitating.
Organics – step 3	10 mL ammonium acetate in 20% (v/v) nitric acid + 30 mg of sodium citrate	Dilute total volume to 40 mL with 18.2 MΩ water. Agitate at room temperature for 30 minutes.
Final step	20 mL 0.3M HF-0.1M HCl	Agitate at room temperature for 4 hours.

Reagent volumes are given for 2g of sample.

Table 4. Calculated ^{234}Th recoil lengths for U-bearing mineral phases and common minerals

Mineral	**^{234}Th recoil length (nm)**
UO_2	14.7[a] – 13.7[b]
Zircon	19.2[a] – 22.7[b]
Quartz	28.8[a]
Apatite	26.8[b]
Monazite	21.5[b]
Muscovite	28.8[b]
Phlogopite	29.5[c]
Albite	30.0[d]
Calcite	29.8[d]
Kaolinite	30.0[d]
Gibbsite	36.9[d]

[a] calculated as in Hashimoto et al. (1985); [b] calculated with the SRIM 2012 software (Ziegler et al., 1996); [c] theoretical value from Jonckheere and Gögen (2001); [d] calculated with the SRIM software in Maher et al. (2006a).

Table 5. Parameters used for *in situ*-produced cosmogenic nuclife models

Parameter	**Description**	**Units**
C	Concentration of *in situ*-produced cosmogenic nuclide	atoms.g^{-1}
C_{tot}	Total nuclide concentration in sediment archive	atoms.g^{-1}
C_{in}	Inherited nuclide concentration	atoms.g^{-1}
C_{deo}	Post-depositional nuclide concentration	atoms.g^{-1}
$P_{(0)}$	Production rate of cosmogenic nuclide	atoms.g^{-1}.yr^{-1}
t	Time since deposition of the sediment	yr
λ	Decay constant of cosmogenic nuclide	yr^{-1}
ε	Erosion rate	cm.yr^{-1}
ρ	Density	g.m^{-3}
Λ	Attenuation length	g.m^{-2}

Table 6. Simplified summary of selected works studying the impact of past climate change on erosion

Reference	**Region**	**Timescale**	**Driver**	**Impact on erosion**	**Comments**
(Burbank et al., 1993)	Himalaya	<10 Myr	+ monsoon	- erosion	Monsoon intensification at 8 Myr suggested to result in reduced mechanical weathering.
(Derry and France-Lanord, 1996)	Himalaya	<20 Myr	+ monsoon	- erosion	Monsoon intensification between 7 and 1Myr, at a time of more intense chemical weathering and reduced physical erosion.
(Clift, 2006)	Himalaya	<20 Myr	+ temperature, moisture	+ erosion	Erosion promoted during warm, humid mid-Miocene.
(Bookhagen et al., 2006)	Himalaya	Early Holocene	+ monsoon	+ erosion	
(Clift et al., 2008)	Himalaya	<15 kyr	+ monsoon	+ erosion	Erosion of the Lesser Himalaya triggered by monsoon intensification at 14 kyr.
(Willenbring and Von Blanckenburg, 2010)	Global	<10 Myr	Glacial cycles	No changes in erosion and weathering	
(Hu et al., 2012)	Taiwan	<14 kyr	+ monsoon	+ erosion	Intensification of the monsoon at 14 kyr results in more active erosion in Taiwan.
(Uba et al., 2007)	Andes	<5 Myr	+ monsoon	+ sediment accumulation	
Cosmogenic nuclide studies					
(Schaller et al., 2002)	Western Europe	<30 kyr	Deglaciation	- erosion	
(Fuller et al., 2009)	Western USA	<30 kyr	- temperature	+ erosion	Highest erosion rates during the late Pleistocene (20-30 kyr ago) interpreted as correlating with

					increased precipitation.
(Schaller et al., 2004)	Western Europe	<1.3 Myr	+ amplitude and duration of climatic cycles, + uplift	+ erosion	
(McPhillips et al., 2013)	Peru	0-16 kyr	+ rainfall	+ erosion	
(Bekaddour et al., 2014)	Peru	<50 kyr	+ rainfall	+ erosion	
(Hidy et al., 2014)	Texas, USA	<500 kyr	+ temperature	+ erosion	
(Balco and Stone, 2005)	Western USA	0.6-0.7 Myr	Basin subsidence	+ erosion	No relationship between climatic cycles and erosion rates.
(Charreau et al., 2011)	Tibet	<9 Myr	Onset of glaciations	+ erosion	
Uranium isotope studies					
(DePaolo et al., 2006)	North Atlantic	<400 kyr	Glaciations	+ regolith residence time	Erosion of exposed continental shelves, where sediment is stored for extensive periods of time.
(Dosseto et al., 2010)	Southeastern Australia	<100 kyr	Climate and vegetation	shorter residence time during drier periods with sparse vegetation	Vegetation change in the regolith source region (shrubs) promotes active erosion of upland soils.

References

Abbott, L.D., Silver, E.A., Anderson, R.S., Smith, R., Ingle, J.C., King, K.A., Haig, D.W., Small, E.E., Galewsky, J. and Sliter, W.V., 1997. Measurement of tectonic surface uplift in a young collisional mountain belt. Nature, 385: 501-507.

Aciego, S., Bourdon, B., Schwander, J., Baur, H. and Forieri, A., 2011. Toward a radiometric ice clock: uranium ages of the Dome C ice core. Quaternary Science Reviews, 30(19-20): 2389-2397.

Acosta, V.T., Schildgen, T.F., Clarke, B.A., Scherler, D., Bookhagen, B., Wittmann, H., von Blanckenburg, F. and Strecker, M.R., 2015. Effect of vegetation cover on millennial-scale landscape denudation rates in East Africa. Lithosphere: L402. 1.

Adam, D.P. and West, G.J., 1983. Temperature and precipitation estimates through the last glacial cycle from Clear Lake, California, pollen data. Science, 219(4581): 168-170.

Adloff, J.P. and Roessler, K., 1991. Recoil and transmutation effects in the migration behaviour of actinides. Radiochim. Acta, 52/53: 269-274.

Andersen, M.B., Erel, Y. and Bourdon, B., 2009. Experimental evidence for 234U–238U fractionation during granite weathering with implications for 234U/238U in natural waters. Geochimica et Cosmochimica Acta, 73(14): 4124-4141.

Anderson, R.S., Repka, J.L. and Dick, G.S., 1996. Explicit treatment of inheritance in dating depositional surfaces using in situ ^{10}Be and ^{26}Al. Geology, 24(1): 47-51.

Avnir, D. and Jaroniec, M., 1989. An isotherm equation for adsorption on fractal surfaces of heterogeneous porous materials. Langmuir, 5(6): 1431-1433.

Bacon, A.R., Richter, D.d., Bierman, P.R. and Rood, D.H., 2012. Coupling meteoric 10Be with pedogenic losses of 9Be to improve soil residence time estimates on an ancient North American interfluve. Geology, 40(9): 847-850.

Balco, G. and Rovey, C.W., 2008. An isochron method for cosmogenic-nuclide dating of buried soils and sediments. American Journal of Science, 308(10): 1083-1114.

Balco, G., Stone, J.O., Lifton, N.A. and Dunai, T.J., 2008. A complete and easily accessible means of calculating surface exposure ages or erosion rates from 10 Be and 26 Al measurements. Quaternary geochronology, 3(3): 174-195.

Balco, G. and Stone, J.O.H., 2005. Measuring middle Pleistocene erosion rates with cosmic-ray-produced nuclides in buried alluvial sediment, Fisher Valley, southeastern Utah. Earth Surface Processes and Landforms.

Banerjee, D., Page, K. and Lepper, K., 2002. Optical dating of palaeochannel deposits in the riverine plain, southeastern Australia: Testing the reliability of existing thermoluminescence dates. Radiation Protection Dosimetry, 101(1-4): 327-332.

Barrows, T.T., Lehman, S.J., Fifield, L.K. and De Deckker, P., 2007. Absence of Cooling in New Zealand and the Adjacent Ocean During the Younger Dryas Chronozone. Science, 318(5847): 86-89.

Bekaddour, T., Schlunegger, F., Vogel, H., Delunel, R., Norton, K.P., Akçar, N. and Kubik, P., 2014. Paleo erosion rates and climate shifts recorded by Quaternary cut-and-fill sequences in the Pisco valley, central Peru. Earth and Planetary Science Letters, 390: 103-115.

Bierman, P.R., 1994. Using in situ produced cosmogenic isotopes to estimate rates of landscape evolution: A review from the geomorphic perspective. J. Geophys. Res., 99(B7): 13885-13896.

Bierman, P.R. and Nichols, K.K., 2004. Rock to sediment - slope to sea with ^{10}Be - rates of landscape change. Annu. Rev. Earth Planet. Sci., 32: 215-255.

Bierman, P.R. and Steig, E.J., 1996. Estimating rates of denudation using cosmogenic isotope abundances in sediment. Earth Surf. Proc. Landforms, 21: 125-139.

Blodgett, T.A. and Isacks, B.L., 2007. Landslide erosion rate in the Eastern Cordillera of Northern Bolivia. Earth Interactions, 11(19): 1-30.

Blum, M.D. and Valastro, S., 1989. Response of the Pedernales River of central Texas to late Holocene climatic change. Annals of the Association of American Geographers, 79(3): 435-456.

Bookhagen, B., Fleitmann, D., Nishiizumi, K., Strecker, M.R. and Thiede, R.C., 2006. Holocene monsoonal dynamics and fluvial terrace formation in the northwest Himalaya, India. Geology, 34(7): 601-604.

Bookhagen, B. and Strecker, M.R., 2012. Spatiotemporal trends in erosion rates across a pronounced rainfall gradient: Examples from the southern Central Andes. Earth and Planetary Science Letters, 327–328(0): 97-110.

Bookhagen, B., Thiede, R.C. and Strecker, M.R., 2005a. Abnormal monsoon years and their control on erosion and sediment flux in the high, arid northwest Himalaya. Earth and Planetary Science Letters, 231(1–2): 131-146.

Bookhagen, B., Thiede, R.C. and Strecker, M.R., 2005b. Late Quaternary intensified monsoon phases control landscape evolution in the northwest Himalaya. Geology, 33(2): 149-152.

Bourdon, B., Bureau, S., Andersen, M.B., Pili, E. and Hubert, A., 2009. Weathering rates from top to bottom in a carbonate environment. Chemical Geology, 258(3-4): 275-287.

Brakenridge, G.R., 1980. Widespread episodes of stream erosion during the Holocene and their climatic cause. Nature, 283: 655-656.

Braucher, R., Brown, E.T., Bourlès, D.L. and Colin, F., 2003. In situ produced Be-10 measurements at great depths: implications for production rates by fast muons. Earth and Planetary Science Letters, 211(3-4): 251-258.

Brown, E.T., Stallard, R.F., Larsen, M.C., Raisbeck, G.M. and Yiou, F., 1995. Denudation rates determined from the accumulation of in-situ produced 10Be in the Luquillo Experimental Forest, Puerto Rico. Earth and Planetary Science Letters, 129: 193-202.

Brunauer, S., Emmett, P.H. and Teller, E., 1938. Adsorption of Gases in Multimolecular Layers. Journal of the American Chemical Society, 60(2): 309-319.

Burbank, D.W., Derry, L.A. and France-Lanord, C., 1993. Reduced Himalayan sediment production 8 Myr ago despite an intensified monsoon. Nature, 364(6432): 48-50.

Burbank, D.W., Leland, J., Fielding, E., Anderson, R.S., Brozovic, N., Reid, M.R. and Duncan, C., 1996. Bedrock incision, rock uplift and threshold hillslopes in the northwestern Himalayas. Nature, 379(6565): 505-510.

Carretier, S., Regard, V., Vassallo, R., Aguilar, G., Martinod, J., Riquelme, R., Pepin, E., Charrier, R., Hérail, G., Farías, M., Guyot, J.-L., Vargas, G. and Lagane, C., 2013. Slope and climate variability control of erosion in the Andes of central Chile. Geology, 41(2): 195-198.

Chabaux, F., Blaes, E., Granet, M., Roupert, R.d.C. and Stille, P., 2012. Determination of transfer time for sediments in alluvial plains using 238U-234U-230Th disequilibria: The case of the Ganges river system. Comptes Rendus Geoscience, 344(11–12): 688-703.

Chabaux, F., Blaes, E., Stille, P., di Chiara Roupert, R., Pelt, E., Dosseto, A., Ma, L., Buss, H.L. and Brantley, S.L., 2013. Regolith formation rate from U-series nuclides: Implications from the study of a spheroidal weathering profile in the Rio Icacos watershed (Puerto Rico). Geochimica et Cosmochimica Acta, 100(0): 73-95.

Chabaux, F., Bourdon, B. and Riotte, J., 2008. U-Series Geochemistry in Weathering Profiles, River Waters and Lakes, Radioactivity in the Environment. Elsevier.

Chabaux, F., Granet, M., Pelt, E., France-Lanord, C. and Galy, V., 2006. ^{238}U-^{234}U-^{230}Th disequilibria and timescale of sedimentary transfers in rivers: Clues from the Gangetic plain rivers. Journal of Geochemical Exploration, 88(1-3): 373-375.

Chabaux, F., Riotte, J. and Dequincey, O., 2003. U-Th-Ra fractionation during weathering and river transport. In: B. Bourdon, G.M. Henderson, C.C. Lundstrom and S.P. Turner (Editors), Uranium-series Geochemistry. Reviews in Mineralogy and Geochemistry. Geochemical Society - Mineralogical Society of America, Washington, pp. 533-576.

Charreau, J., Blard, P.H., Puchol, N., Avouac, J.P., Lallier-Vergès, E., Bourlès, D., Braucher, R., Gallaud, A., Finkel, R., Jolivet, M., Chen, Y. and Roy, P., 2011. Paleo-erosion rates in Central Asia since 9Ma: A transient increase at the onset of Quaternary glaciations? Earth and Planetary Science Letters, 304(1-2): 85-92.

Christl, M., Wieler, R. and Finkel, R.C., 2014. Measuring one atom in a million billion with mass spectrometry.

Clapp, E.M., Bierman, P.R. and Caffee, M., 2002. Using 10 Be and 26 Al to determine sediment generation rates and identify sediment source areas in an arid region drainage basin. Geomorphology, 45(1): 89-104.

Clift, P.D., 2006. Controls on the erosion of Cenozoic Asia and the flux of clastic sediment to the ocean. Earth and Planetary Science Letters, 241(3–4): 571-580.

Clift, P.D., Giosan, L., BIusztajn, J., Campbell, I.H., Allen, C., Pringle, M., Tabrez, A.R., Danish, M., Rabbani, M.M., Alizai, A., Carter, A. and Lueckge, A., 2008. Holocene erosion of the Lesser Himalaya triggered by intensified summer monsoon. Geology, 36(1): 79-82.

Codilean, A.T., Fenton, C.R., Fabel, D., Bishop, P. and Xu, S., 2012. Discordance between cosmogenic nuclide concentrations in amalgamated sands and individual fluvial pebbles in an arid zone catchment. Quaternary Geochronology.

Cohen, S., Willgoose, G. and Hancock, G., 2013. Soil–landscape response to mid and late Quaternary climate fluctuations based on numerical simulations. Quaternary Research, 79(3): 452-457.

Coulthard, T., Kirkby, M. and Macklin, M., 2000. Modelling geomorphic response to environmental change in an upland catchment. Hydrological Processes, 14(11-12): 2031-2045.

Covault, J., Craddock, W., Romans, B., Fildani, A. and Gosai, M., 2013. Spatial and temporal variations in landscape evolution: Historic and longer-term sediment flux through global catchments. The Journal of Geology, 121(1): 35-56.

Cyr, A.J. and Granger, D.E., 2008. Dynamic equilibrium among erosion, river incision, and coastal uplift in the northern and central Apennines, Italy. Geology, 36(2): 103-106.

Davis, M., Matmon, A., Rood, D.H. and Avnaim-Katav, S., 2012. Constant cosmogenic nuclide concentrations in sand supplied form the Nile River over the past 2.5 m.y. Geology, 40: 359-362.

Delunel, R., Bourlès, D.L., van der Beek, P.A., Schlunegger, F., Leya, I., Masarik, J. and Paquet, E., 2014. Snow shielding factors for cosmogenic nuclide dating inferred from long-term neutron detector monitoring. Quaternary Geochronology, 24: 16-26.

DePaolo, D.J., Lee, V.E., Christensen, J.N. and Maher, K., 2012. Uranium comminution ages: Sediment transport and deposition time scales. Comptes Rendus Geoscience, 344(11–12): 678-687.

DePaolo, D.J., Maher, K., Christensen, J.N. and McManus, J., 2006. Sediment transport time measured with U-series isotopes: Results from ODP North Atlantic drift site 984. Earth and Planetary Science Letters, 248(1-2): 394-410.

Derry, L.A. and France-Lanord, C., 1996. Neogene Himalayan weathering history and river $^{87}Sr/^{86}Sr$: impact on the marine Sr record. Earth and Planetary Science Letters, 142(1–2): 59-74.

Desilets, D., Zreda, M. and Prabu, T., 2006. Extended scaling factors for in situ cosmogenic nuclides: new measurements at low latitude. Earth and Planetary Science Letters, 246(3): 265-276.

Dosseto, A., 2015. Chemical Weathering (U-Series). Encyclopedia of Scientific Dating Methods: 152-169.

Dosseto, A., Bourdon, B., Gaillardet, J., Allègre, C.J. and Filizola, N., 2006a. Timescale and conditions of chemical weathering under tropical climate: Study of the Amazon basin with U-series. Geochim. Cosmochim. Acta, 70(1): 71-89.

Dosseto, A., Bourdon, B., Gaillardet, J., Maurice-Bourgoin, L. and Allègre, C.J., 2006b. Weathering and transport of sediments in the Bolivian Andes: time constraints from uranium-series isotopes. Earth and Planetary Science Letters, 248(3-4): 759-771.

Dosseto, A., Bourdon, B. and Turner, S.P., 2008a. Uranium-series isotopes in river materials: Insights into the timescales of erosion and sediment transport. Earth and Planetary Science Letters, 265(1-2): 1-17.

Dosseto, A., Buss, H.L. and Suresh, P.O., 2012. Rapid regolith formation over volcanic bedrock and implications for landscape evolution. Earth and Planetary Science Letters, 337–338(0): 47-55.

Dosseto, A., Hesse, P., Maher, K., Fryirs, K. and Turner, S.P., 2010. Climatic and vegetation control on sediment dynamics. Geology, 38: 395-398.

Dosseto, A. and Riebe, C.S., 2011. Inception! Timescale of Chemical Weathering during the Early Stages of Water-Rock Interaction. Mineralogical Magazine, 75(3): 776.

Dosseto, A., Turner, S.P. and Chappell, J., 2008b. The evolution of weathering profiles through time: New insights from uranium-series isotopes. Earth and Planetary Science Letters, 274(3-4): 359-371.

Dühnforth, M., Anderson, R.S., Ward, D. and Stock, G.M., 2010. Bedrock fracture control of glacial erosion processes and rates. Geology, 38(5): 423-426.

Dunai, T.J., 2000. Scaling factors for production rates of in situ produced cosmogenic nuclides: a critical reevaluation. Earth and Planetary Science Letters, 176(1): 157-169.

Dunne, A., Elmore, D. and Muzikar, P., 1999. Scaling factors for the rates of production of cosmogenic nuclides for geometric shielding and attenuation at depth on sloped surfaces. Geomorphology, 27(1-2): 3-11.

Erlanger, E.D., Granger, D.E. and Gibbon, R.J., 2012. Rock uplift rates in South Africa from isochron burial dating of fluvial and marine terraces. Geology, 40(11): 1019-1022.

Fleischer, R.L., 1980. Isotopic disequilibrium of uranium: Alpha-recoil damage and preferential solution effects. Science, 207(4434): 979-981.

Fleischer, R.L., 1982. Nature of alpha-recoil damage: Evidence from preferential solution effects. Nuclear Tracks and Radiation Measurements (1982), 6(1): 35-42.

Fuller, T.K., Perg, L.A., Willenbring, J.K. and Lepper, K., 2009. Field evidence for climate-driven changes in sediment supply leading to strath terrace formation. Geology, 37(5): 467-470.

Godard, V., Burbank, D.W., Bourlès, D.L., Bookhagen, B., Braucher, R. and Fisher, G.B., 2012. Impact of glacial erosion on 10Be concentrations in fluvial sediments of the Marsyandi catchment, central Nepal. Journal of Geophysical Research, 117(F3).

Godard, V., Tucker, G.E., Burch Fisher, G., Burbank, D.W. and Bookhagen, B., 2013. Frequency-dependent landscape response to climatic forcing. Geophysical Research Letters, 40(5): 859-863.

Gosse, J.C. and Phillips, F.M., 2001. Terrestrial in situ cosmogenic nuclides: theory and application. Quaternary Science Reviews, 20(14): 1475-1560.

Granet, M., Chabaux, F., Stille, P., Dosseto, A., France-Lanord, C. and Blaes, E., 2010. U-series disequilibria in suspended river sediments and implication for sediment transfer time in alluvial plains: The case of the Himalayan rivers. Geochimica et Cosmochimica Acta, 74: 2851-2865.

Granet, M., Chabaux, F., Stille, P., France-Lanord, C. and Pelt, E., 2007. Time-scales of sedimentary transfer and weathering processes from U-series nuclides: Clues from the Himalayan rivers. Earth and Planetary Science Letters, 261(3-4): 389-406.

Granger, D., 2014. Cosmogenic nuclide burial dating in archaeology and paleoanthropology. Treatise on Geochemistry, Second Edition. Oxford: Elsevier, 14: 81-97.

Granger, D.E., Fabel, D. and Palmer, A.N., 2001. Pliocene− Pleistocene incision of the Green River, Kentucky, determined from radioactive decay of cosmogenic 26Al and 10Be in Mammoth Cave sediments. Geological Society of America Bulletin, 113(7): 825-836.

Granger, D.E., Kirchner, J.W. and Finkel, R., 1996. Spatially averaged long-term erosion rates measured from in-situ produced cosmogenic nuclides in alluvial sediment. J. Geol., 104: 249-257.

Granger, D.E., Kirchner, J.W. and Finkel, R.C., 1997. Quaternary downcutting rate of the New River, Virginia, measured from differential decay of cosmogenic 26Al and 10Be in cave-deposited alluvium. Geology, 25(2): 107-110.

Granger, D.E., Lifton, N.A. and Willenbring, J.K., 2013. A cosmic trip: 25 years of cosmogenic nuclides in geology. Geological Society of America Bulletin, 125(9-10): 1379-1402.

Granger, D.E. and Muzikar, P.F., 2001. Dating sediment burial with in situ-produced cosmogenic nuclides: theory, techniques, and limitations. Earth and Planetary Science Letters, 188(1-2): 269-281.

Granger, D.E. and Schaller, M., 2014. Cosmogenic nuclides and erosion at the watershed scale. Elements, 10(5): 369-373.

Granger, D.E. and Smith, A.L., 2000. Dating buried sediments using radioactive decay and muogenic production of 26Al and 10Be. Nuclear instruments and methods in physics research section B: beam interactions with materials and atoms, 172(1): 822-826.

Handley, H.K., Turner, S., Afonso, J.C., Dosseto, A. and Cohen, T., 2013a. Sediment residence times constrained by uranium-series isotopes: A critical appraisal of the comminution approach. Geochimica et Cosmochimica Acta, 103(0): 245-262.

Handley, H.K., Turner, S., Dosseto, A., Haberlah, D., Afonso, J.C. and Schaefer, B., 2013b. Considerations for the determination of sediment residence times using the uranium-isotope comminution method: insights from palaeochannel deposits and bedrock of South Australia. Chem. Geol., 340: 40-48.

Hashimoto, T., Aoyagi, Y., Kudo, H. and Sotobayashi, T., 1985. Range calculation of alpha-recoil atoms in some minerals using LSS-theory. Journal of Radioanalytical and Nuclear Chemistry, 90(2): 415-438.

Heimsath, A.M., Dietrich, W.E., Nishiizumi, K. and Finkel, R., 1997. The soil production function and landscape equilibrium. Nature, 388: 358-361.

Herman, F., Seward, D., Valla, P.G., Carter, A., Kohn, B., Willett, S.D. and Ehlers, T.A., 2013. Worldwide acceleration of mountain erosion under a cooling climate. Nature, 504(7480): 423-6.

Heusser, L.E. and van de Geer, G., 1994. Direct correlation of terrestrial and marine paleoclimatic records from four glacial-interglacial cycles -- DSDP site 594 Southwest Pacific. Quaternary Science Reviews, 13(3): 273-282.

Hidy, A.J., Gosse, J.C., Blum, M.D. and Gibling, M.R., 2014. Glacial–interglacial variation in denudation rates from interior Texas, USA, established with cosmogenic nuclides. Earth and Planetary Science Letters, 390: 209-221.

Hinderer, M. and Einsele, G., 2001. The world's large lake basins as denudation-accumulation systems and implications of their lifetimes. Journal of Paleolimnology, 26(4): 355-372.

Hippe, K., Kober, F., Zeilinger, G., Ivy-Ochs, S., Maden, C., Wacker, L., Kubik, P.W. and Wieler, R., 2012. Quantifying denudation rates and sediment storage on the eastern Altiplano, Bolivia, using cosmogenic 10 Be, 26 Al, and in situ 14 C. Geomorphology, 179: 58-70.

Hu, D., Böning, P., Köhler, C.M., Hillier, S., Pressling, N., Wan, S., Brumsack, H.J. and Clift, P.D., 2012. Deep sea records of the continental weathering and erosion response to East Asian monsoon intensification since 14 ka in the South China Sea. Chemical Geology, 326–327(0): 1-18.

Hussain, N. and Lal, D., 1986. Preferential solution of ^{234}U from recoil tracks and ^{234}U/^{238}U radioactive disequilibrium in natural waters. Proceedings of the Indian Academy of Sciences - Earth and Planetary Sciences, 95(2): 245-263.

Istanbulluoglu, E. and Bras, R.L., 2005. Vegetation-modulated landscape evolution: Effects of vegetation on landscape processes, drainage density, and topography. Journal of Geophysical Research: Earth Surface (2003–2012), 110(F2).

Jerolmack, D.J. and Paola, C., 2010. Shredding of environmental signals by sediment transport. Geophysical Research Letters, 37(19): n/a-n/a.

Jonckheere, R. and Gögen, K., 2001. A Monte-Carlo calculation of the size distribution of latent alpha-recoil tracks. Nuclear Instruments and Methods in Physics Research Section B: Beam Interactions with Materials and Atoms, 183(3–4): 347-357.

Kershaw, A.P., 1986. Climatic change and Aboriginal burning in north-east Australia during the last two glacial/interglacial cycles. Nature, 322(6074): 47-49.

Kershaw, A.P., McKenzie, G.M., Porch, N., Roberts, R.G., Brown, J., Heijnis, H., Orr, M.L., Jacobsen, G. and Newall, P.R., 2007. A high-resolution record of vegetation and climate through the last glacial cycle from Caledonia Fen, southeastern highlands of Australia. Journal of Quaternary Science, 22(5): 481-500.

Kigoshi, K., 1971. Alpha-recoil thorium-234: Dissolution into water and the uranium-234/uranium-238 disequilibrium in nature. Science, 173(3991): 47-48.

Knox, J.C., 1972. VALLEY ALLUVIATION IN SOUTHWESTERN WISCONSIN. Annals of the Association of American Geographers, 62(3): 401-410.

Kohl, C.P. and Nishiizumi, K., 1992. Chemical isolation of quartz for measurement of in-situ -produced cosmogenic nuclides. Geochimica et Cosmochimica Acta, 56(9): 3583-3587.

Lal, D., 1991. Cosmic ray labeling of erosion surfaces: in situ nuclide production rates and erosion models. Earth and Planetary Science Letters, 104(2-4): 424-439.

Landström, O., Tullborg, E.-L. and Eriksson, G., 2001. Effect of glacial/post-glacial weathering compared with hydrothermal alteration - implications for matrix diffusion, Swedish Nuclear Fuel and Waste Management Co.

Langbein, W.B. and Schumm, S.A., 1958. Yield of sediment in relation to mean annual precipitation. Eos, Transactions American Geophysical Union, 39(6): 1076-1084.

Latham, A.G. and Schwarcz, H.P., 1987. On the possibility of determining rates of removal of uranium from crystalline igneous rocks using U-series disequilibria—1: a U-leach model, and its applicability to whole-rock data. Applied Geochemistry, 2(1): 55-65.

Lee, V., DePaolo, D.J. and Christensen, J.N., 2010. Uranium-series comminution ages of continental sediments: Case study of a Pleistocene alluvial fan. Earth and Planetary Science Letters, 296(3-4): 244-254.

Lee, V.E., 2009. Radiogenic isotope geochemistry and the evolution of the Earth's surface and interior, University of California, Berkeley.

Lifton, N.A., Bieber, J.W., Clem, J.M., Duldig, M.L., Evenson, P., Humble, J.E. and Pyle, R., 2005. Addressing solar modulation and long-term uncertainties in scaling secondary cosmic rays for in situ cosmogenic nuclide applications. Earth and Planetary Science Letters, 239(1): 140-161.

Luo, S., Ku, T.-L., Roback, R., Murrell, M. and McLing, T.L., 2000. In-situ radionuclide transport and preferential groundwater flows at INEEL (Idaho): decay-series disequilibrium studies. Geochimica et Cosmochimica Acta, 64(5): 867-881.

Lupker, M., Blard, P.-H., Lavé, J., France-Lanord, C., Leanni, L., Puchol, N., Charreau, J. and Bourlès, D., 2012. ^{10}Be-derived Himalayan denudation rates and sediment budgets in the Ganga basin. Earth and Planetary Science Letters, 333–334(0): 146-156.

Ma, L., Chabaux, F., Pelt, E., Blaes, E., Jin, L. and Brantley, S.L., 2010. Regolith production rates calculated with uranium-series isotopes at Susquehanna/Shale Hills Critical Zone Observatory. Earth and Planetary Science Letters, 297(1-2): 211-255.

Maher, K., DePaolo, D.J. and Christensen, J.N., 2006a. U-Sr isotopic speedometer: Fluid flow and chemical weathering rates in aquifers. Geochimica et Cosmochimica Acta, 70(17): 4417-4435.

Maher, K., DePaolo, D.J. and Lin, J.C.F., 2004. Rates of silicate dissolution in deep-sea sediment: in situ measurement using U-234/U-238 of pore fluids. Geochim. Cosmochim. Acta, 68: 4629-4648.

Maher, K., Steefel, C.I., DePaolo, D.J. and Viani, B.E., 2006b. The mineral dissolution rate conundrum: Insights from reactive transport modeling of U isotopes and pore fluid chemistry in marine sediments. Geochimica et Cosmochimica Acta, 70(2): 337-363.

Marshall, J.A., Roering, J.J., Bartlein, P.J., Gavin, D.G., Granger, D.E., Rempel, A.W., Praskievicz, S.J. and Hales, T.C., 2015. Frost for the trees: Did climate increase erosion in unglaciated landscapes during the late Pleistocene? Science advances, 1(10): e1500715.

Martin, A.N., Dosseto, A. and Kinsley, L.P.J., 2015. Evaluating the removal of non-detrital matter from soils and sediment using uranium isotopes. Chemical Geology, 396(0): 124-133.

Masarik, J., Frank, M., Schäfer, J.M. and Wieler, R., 2001. Correction of in situ cosmogenic nuclide production rates for geomagnetic field intensity variations during the past 800,000 years. Geochimica and Cosmochimica Acta, 65(17): 2995-3003.

Masarik, J. and Reedy, R.C., 1995. Terrestrial cosmogenic-nuclide production systematics calculated from numerical simulations. Earth and Planetary Science Letters, 136(3-4): 381-395.

Matmon, A., Bierman, P.R., Larsen, J., Southworth, S., Pavich, M. and Caffee, M., 2003a. Temporally and spatially uniform rates of erosion in the southern Appalachian Great Smoky Mountains. Geology, 31(2): 155-158.

Matmon, A., Bierman, P.R., Larsen, J., Southworth, S., Pavich, M., Finkel, R. and Caffee, M., 2003b. Erosion of an ancient mountain range, the Great Smoky Mountains, North Carolina and Tennessee. American Journal of Science, 303(9): 817-855.

McPhillips, D., Bierman, P.R., Crocker, T. and Rood, D.H., 2013. Landscape response to Pleistocene-Holocene precipitation change in the Western Cordillera, Peru: 10Be concentrations in modern sediments and terrace fills. Journal of Geophysical Research: Earth Surface, 118(4): 2488-2499.

Métivier, F., Gaudemer, Y., Tapponnier, P. and Klein, M., 1999. Mass accumulation rates in Asia during the Cenozoic. Geophysical Journal International, 137(2): 280-318.

Milliman, J.D. and Syvitski, J.P.M., 1992. Geomorphic/tectonic control of sediment discharge to the ocean: the importance of small mountainous rivers. Journal of Geology, 100(5): 525-544.

Molnar, P., 2004. Late Cenozoic Increase in Accumulation Rates of Terrestrial Sediment: How Might Climate Change Have Affected Erosion Rates? Annual Review of Earth and Planetary Sciences, 32(1): 67-89.

Mudelsee, M. and Schulz, M., 1997. The Mid-Pleistocene climate transition: onset of 100 ka cycle lags ice volume build-up by 280 ka. Earth and Planetary Science Letters, 151: 117-123.

Nichols, K.K., Bierman, P.R. and Rood, D.H., 2014. ^{10}Be constrains the sediment sources and sediment yields to the Great Barrier Reef from the tropical Barron River catchment, Queensland, Australia. Geomorphology, 224(0): 102-110.

Niemi, N.A., Oskin, M., Burbank, D.W., Heimsath, A.M. and Gabet, E.J., 2005. Effects of bedrock landslides on cosmogenically determined erosion rates. Earth and Planetary Science Letters, 237(3-4): 480-498.

Nishiizumi, K., Winterer, E.L., Kohl, C.P. and Klein, J., 1989. Cosmic Ray Production Rates of ^{10}Be and ^{26}Al in Quartz From Glacially Polished Rocks. Journal of Geophysical Research, 94(B12): 17907-17915.

Page, K., Nanson, G. and Price, D., 1996. Chronology of Murrumbidgee River palaeochannels on the Riverine Plain, southeastern Australia. Journal of Quaternary Science, 11(4): 311-326.

Philpotts, A.R., 1990. Principles of Igneous and Metamorphic Petrology. Prentice Hall, 498 pp.

Portenga, E.W. and Bierman, P.R., 2011. Understanding Earth’s eroding surface with 10 Be. GSA Today, 21(8): 4-10.

Putnam, A., Schaefer, J., Barrell, D., Vandergoes, M., Denton, G., Kaplan, M., Finkel, R., Schwartz, R., Goehring, B. and Kelley, S., 2010. In situ cosmogenic 10 Be production-rate calibration from the Southern Alps, New Zealand. Quaternary Geochronology, 5(4): 392-409.

Refsnider, K.A., 2010. Dramatic increase in late Cenozoic alpine erosion rates recorded by cave sediment in the southern Rocky Mountains. Earth and Planetary Science Letters, 297(3–4): 505-511.

Reusser, L.J. and Bierman, P.R., 2010. Using meteoric 10Be to track fluvial sand through the Waipaoa River basin, New Zealand. Geology, 38(1): 47-50.

Riebe, C.S., Kirchner, J.W. and Granger, D.E., 2001. Quantifying quartz enrichment and its consequences for cosmogenic measurements of erosion rates from alluvial sediment and regolith. Geomorphology, 40(1-2): 15-19.

Riebe, C.S., Kirchner, J.W., Granger, D.E. and Finkel, R., 2000. Erosional equilibrium and disequilibrium in the Sierra Nevada, inferred from cosmogenic ^{26}Al and ^{10}Be in alluvial sediment. Geology, 28(9): 803-806.

Rosholt, J., 1982. Mobilization and weathering. In: M. Ivanovich and R.S. Harmon (Editors), Uranium-series disequilibrium: Application to environmental problems. Oxford Sciences Publications, Oxford, pp. 167-180.

Rosholt, J., Doe, B. and Tatsumoto, M., 1966. Evolution of the isotopic composition of uranium and thorium in soil profiles. Geol. Soc. Am. Bull., 77: 987-1004.

Rosholt, J.N., 1983. Isotopic composition of uranium and throium in crystalline rocks. Journal of Geophysical Research, 88(B9): 7315-7330.

Sadler, P.M., 1981. Sediment Accumulation Rates and the Completeness of Stratigraphic Sections. The Journal of Geology, 89(5): 569-584.

Safran, E.B., Bierman, P.R., Aalto, R., Dunne, T., Whipple, K.X. and Caffee, M., 2005. Erosion rates driven by channel network incision in the Bolivian Andes. Earth Surface Processes and Landforms, 30(8): 1007-1024.

Schaller, M. and Ehlers, T.A., 2006. Limits to quantifying climate driven changes in denudation rates with cosmogenic radionuclides. Earth and Planetary Science Letters, 248(1-2): 153-167.

Schaller, M., von Blanckenburg, F., Hovius, N. and Kubik, P.W., 2001. Large-scale erosion rates from in-situ produced cosmogenic nuclides in European river sediments. Earth Planet. Sci. Lett., 188(3-4): 441-458.

Schaller, M., Von Blanckenburg, F., Hovius, N., Veldkamp, A., van der Berg, M.W. and Kubik, P.W., 2004. Paleo-erosion rates from cosmogenic 10Be in a 1.3 Ma terrace sequence: response of the River Meuse to changes in climate and rock uplift rate. J. Geol., 112: 127-144.

Schaller, M., von Blanckenburg, F., Veldkamp, A., Tebbens, L.A., Hovius, N. and Kubik, P.W., 2002. A 30,000 yr record of erosion rates from cosmogenic 10Be in Middle European river terraces. Earth and Planetary Science Letters, 204(1-2): 307-320.

Schildgen, T., Phillips, W. and Purves, R., 2005. Simulation of snow shielding corrections for cosmogenic nuclide surface exposure studies. Geomorphology, 64(1): 67-85.

Schultz, M.K., Burnett, W.C. and Inn, G.W., 1998. Evaluation of a sequential extraction method for determining actinide fractionation in soils and sediments. J. Environ. Radioactivity, 40(2): 155-174.

Scott, R.D., MacKenzie, A.B. and Alexander, W.R., 1992. The interpretation of ^{238}U-^{234}U-^{230}Th-^{226}Ra disequilibria produced by rock-water interactions. Journal of Geochemical Exploration, 45(1-3): 323-343.

Semkow, T.M., 1991. Fractal model of radon emanation from solids. Physical Review Letters, 66(23): 3012-3015.

Shuster, D.L., Ehlers, T.A., Rusmore, M.E. and Farley, K.A., 2005. Geology: Rapid glacial erosion at 1.8 Ma revealed by 4He/ 3He thermochronometry. Science, 310(5754): 1668-1670.

Simpson, G. and Castelltort, S., 2012. Model shows that rivers transmit high-frequency climate cycles to the sedimentary record. Geology, 40(12): 1131-1134.

Small, E.E., Anderson, R.S. and Hancock, G.S., 1999. Estimates of the rate of regolith production using 10Be and 26Al from an alpine hillslope. Geomorphology, 27(1-2): 131-150.

Steffen, D., Schlunegger, F. and Preusser, F., 2009. Drainage basin response to climate change in the Pisco valley, Peru. Geology, 37(6): 491-494.

Stone, J.O., 2000. Air pressure and cosmogenic isotope production. Journal of Geophysical Research, 105(B10): 23,753-23,759.

Stone, J.O., Allan, G.L., Fifield, L.K. and Cresswell, R.G., 1996. Cosmogenic chlorine-36 from calcium spallation. Geochimica et Cosmochimica Acta, 60(4): 679-692.

Summerfield, M.A. and Hulton, N.J., 1994. Natural controls of fluvial denudation rates in major world drainage basin. J. Geophys. Res., 99(B7): 13871-13883.

Sun, H. and Furbish, D.J., 1995. Moisture content effect on radon emanation in porous media. Journal of Contaminant Hydrology, 18(3): 239-255.

Syvitski, J.P.M. and Milliman, J.D., 2007. Geology, geography, and humans battle for dominance over the delivery of fluvial sediment to the coastal ocean. Journal of Geology, 115(1): 1-19.

Tebbens, L.A., Veldkamp, A., Westerhoff, W. and Kroonenberg, S.B., 1999. Fluvial incision and channel downcutting as a response to Lateglacial and early Holocene climate change: the lower reach of the River Meuse (Maas). Journal of Quaternary Science, 14: 59-75.

Tessier, A., Campbell, P.G.C. and Bisson, M., 1979. Sequential extraction procedure for the speciation of particulate trace metals. Analytical Chemistry, 51(7): 844-851.

Thompson, R.S., 1991. Pliocene Environments and Climates in the Western United-States. Quat. Sci. Rev., 10(2-3): 115-132.

Trauth, M.H., Alonso, R.A., Haselton, K.R., Hermanns, R.L. and Strecker, M.R., 2000. Climate change and mass movements in the NW Argentine Andes. Earth and Planetary Science Letters, 179(2): 243-256.

Trauth, M.H., Bookhagen, B., Marwan, N. and Strecker, M.R., 2003. Multiple landslide clusters record Quaternary climate changes in the northwestern Argentine Andes. Palaeogeography, Palaeoclimatology, Palaeoecology, 194(1–3): 109-121.

Tucker, G.E. and Slingerland, R., 1997. Drainage basin responses to climate change. Water Resources Research, 33(8): 2031-2047.

Uba, C.E., Strecker, M.R. and Schmitt, A.K., 2007. Increased sediment accumulation rates and climatic forcing in the central Andes during the late Miocene. Geology, 35(11): 979-982.

Van Balen, R.T., Houtgast, R.F., Van der Wateren, F.M., Vandenberghe, J. and Bogaart, P.W., 2000. Sediment budget and tectonic evolution of the Meuse catchment in the Ardennes and the Roer Valley Rift System. Global and Planetary Change, 27: 113-129.

van den Berg, M.W. and van Hoof, T., 2001. The Maas terrace sequence at Maastricht, SE Netherlands: evidence for 200 m of late Neogene and Quaternary surface uplift. In: D. Maddy, M.G. Macklin and J.C. Woodward (Editors), River Basin Sediment Systems: Archives of Environmental Change. A. A. Balkema Publishers, Lisse, pp. 503.

Veldkamp, A. and Kroonenberg, S., 1993. Late Quaternary chronology of the Allier terrace sediments (Massif Central, France). Geologie en Mijnbouw, 72: 179-192.

Vigier, N. and Bourdon, B., 2011. Constraining Rates of Chemical and Physical Erosion Using U-Series Radionuclides. In: M. Baskaran (Editor), Handbook of Environmental Isotope Geochemistry. Advances in Isotope Geochemistry. Springer Berlin Heidelberg, pp. 553-571.

Vigier, N., Bourdon, B., Lewin, É., Dupré, B., Turner, S., Van Calsteren, P., Subramanian, V. and Allègre, C.J., 2005. Mobility of U-series nuclides during basalt weathering: An example of the Deccan Traps (India). Chem. Geol., 219(1-4): 69-91.

Vigier, N., Bourdon, B., Turner, S. and Allègre, C.J., 2001. Erosion timescales derived from U-decay series measurements in rivers. Earth Planet. Sci. Lett., 193: 546-563.

Vigier, N., Burton, K.W., Gislason, S.R., Rogers, N.W., Duchene, S., Thomas, L., Hodge, E. and Schaefer, B., 2006. The relationship between riverine U-series disequilibria and erosion rates in a basaltic terrain. Earth and Planetary Science Letters, 249(3-4): 258-273.

von Blanckenburg, F., 2006. The control mechanisms of erosion and weathering at basin scale from cosmogenic nuclides in river sediment. Earth and Planetary Science Letters, 242(3-4): 224-239.

von Blanckenburg, F., Bouchez, J. and Wittmann, H., 2012. Earth surface erosion and weathering from the 10Be (meteoric)/9Be ratio. Earth and Planetary Science Letters, 351–352(0): 295-305.

Ward, P.J., van Balen, R.T., Verstraeten, G., Renssen, H. and Vandenberghe, J., 2009. The impact of land use and climate change on late Holocene and future suspended sediment yield of the Meuse catchment. Geomorphology, 103(3): 389-400.

West, N., Kirby, E., Bierman, P., Slingerland, R., Ma, L., Rood, D. and Brantley, S., 2013. Regolith production and transport at the Susquehanna Shale Hills Critical Zone Observatory, Part 2: Insights from meteoric 10Be. Journal of Geophysical Research: Earth Surface, 118(3): 1877-1896.

White, A.F. and Brantley, S.L., 2003. The effect of time on the weathering of silicate minerals: why do weathering rates differ in the laboratory and field? Chemical Geology, 202(3-4): 479-506.

Willenbring, J.K. and Jerolmack, D.J., 2015. The null hypothesis: globally steady rates of erosion, weathering fluxes and shelf sediment accumulation during Late Cenozoic mountain uplift and glaciation. Terra Nova: n/a-n/a.

Willenbring, J.K. and Von Blanckenburg, F., 2010. Long-term stability of global erosion rates and weathering during late-Cenozoic cooling. Nature, 465(7295): 211-214.

Wittmann, H. and von Blanckenburg, F., 2009. Cosmogenic nuclide budgeting of floodplain sediment transfer. Geomorphology, 109(3-4): 246-256.

Wittmann, H., von Blanckenburg, F., Bouchez, J., Dannhaus, N., Naumann, R., Christl, M. and Gaillardet, J., 2012. The dependence of meteoric ^{10}Be concentrations on particle size in Amazon River bed sediment and the extraction of reactive ^{10}Be/ ^{9}Be ratios. Chemical Geology.

Wittmann, H., von Blanckenburg, F., Guyot, J.L., Maurice, L. and Kubik, P.W., 2009. From source to sink: Preserving the cosmogenic 10Be-derived denudation rate signal of the Bolivian Andes in sediment of the Beni and Mamoré foreland basins. Earth and Planetary Science Letters, 288(3-4): 463-474.

Wittmann, H., von Blanckenburg, F., Kruesmann, T., Norton, K.P. and Kubik, P.W., 2007. Relation between rock uplift and denudation from cosmogenic nuclides in river sediment in the Central Alps of Switzerland. Journal of Geophysical Research: Earth Surface (2003–2012), 112(F4).

Wittmann, H., von Blanckenburg, F., Maurice, L., Guyot, J.L., Filizola, N. and Kubik, P.W., 2010. Sediment production and delivery in the Amazon River basin quantified by in situ-produced cosmogenic nuclides and recent river loads. Geological Society of America Bulletin, 123(5-6): 934-950.

Wittmann, H., von Blanckenburg, F., Maurice, L., Guyot, J.L. and Kubik, P.W., 2011. Recycling of Amazon floodplain sediment quantified by cosmogenic 26Al and 10Be. Geology, 39(5): 467-470.

Worm, H.-U., Ahmed, A., Ahmed, N., Islam, H., Huq, M., Hambach, U. and Lietz, J., 1998. Large sedimentation rate in the Bengal Delta: magnetostratigraphic dating of Cenozoic sediments from northeastern Bangladesh. Geology, 26(6): 487-490.

Yanites, B.J., Tucker, G.E. and Anderson, R.S., 2009. Numerical and analytical models of cosmogenic radionuclide dynamics in landslide-dominated drainage basins. Journal of Geophysical Research, 114(F1).

Zhang, P., Molnar, P. and Downs, W.R., 2001. Increased sedimentation rates and grain sizes 2-4 Myr ago due to the influence of climate change on erosion rates. Nature, 410(6831): 891-897.

Ziegler, J.F., Biersack, J.P. and Littmark, U., 1996. The Stopping and Range of Ions in Solids. Pergamon Press, Oxford.